Electron spin relaxation due to small-angle motion: Theory for the canonical orientations and application to hierarchic cage dynamics in ionomers

D. Leporini[a)]
Max-Planck-Institut für Polymerforschung, Postfach 3148, D-55021 Mainz, Germany; Dipartimento di Fisica Enrico Fermi, Universita' di Pisa, Via F. Buonarroti 2, I-56127 Pisa, Italy; and INFM, Via F. Buonarroti 2, I-56127 Pisa, Italy

V. Schädler
Max-Planck-Institut für Polymerforschung, Postfach 3148, D-55021 Mainz, Germany

U. Wiesner
Max-Planck-Institut für Polymerforschung, Postfach 3148, D-55021 Mainz, Germany and Materials Science & Engineering, Cornell University, Ithaca, New York 14853-1501

H. W. Spiess and G. Jeschke
Max-Planck-Institut für Polymerforschung, Postfach 3148, D-55021 Mainz, Germany

(Received 28 May 2003; accepted 11 September 2003)

Analytical expressions for transverse electron spin relaxation induced by small angle motion were derived for the first time within an anisotropic model for rotational diffusion by using an approximation of the spin Hamiltonian and its variation during reorientation that is valid close to the canonical orientations. The dependence of the decay of the stimulated echo on such motion was studied by extensive Monte Carlo simulations and regimes were identified in which the time constant of this decay is related to parameters of the anisotropic diffusion model by simple equations. For testing these theoretical findings and obtaining insight into hierarchical cage dynamics in soft matter, high-field electron paramagnetic resonance (EPR) measurements were performed at a frequency of 94 GHz where the canonical orientations for nitroxide spin labels are well resolved. A combination of continuous wave EPR, saturation recovery measurements, and measurements of the decay of primary and stimulated electron spin echoes was employed to cover time scales from a few picoseconds up to several microseconds. Ionic spin probes attached by electrostatic interactions to the surface of ionic clusters in ionomers were used as a model system in which slow cage reorientation can be studied in the glass transition region of the polymer ($0.64 < T/T_g < 1.05$). Three hierarchical reorientation processes of the spin probe were observed on different time scales. The spin probe undergoes fast intramolecular libration on the time scale of a few picoseconds, it experiences a local rearrangement of the cage on the time scale of hundreds of nanoseconds and it performs cooperative reorientation coupled to the structural relaxation of the glassy matrix over time scales comparable to or longer than several microseconds in the glass transition region. © *2003 American Institute of Physics.* [DOI: 10.1063/1.1623479]

I. INTRODUCTION

Molecular reorientation in disordered systems like amorphous polymers or low molecular mass glass formers occurs on different time scales as it is observed by nuclear magnetic resonance (NMR)[1] dielectric[2–5] and mechanical[6] relaxation, and optical spectroscopy.[7,8] On approaching the glass transition, the large-scale motion becomes more and more impeded by the increasing structural constraints.[9–12] Molecules, or subunits of macromolecules, are surrounded and trapped by rigid pockets, which are usually referred to as cages. The cage effect can be imaged in real space by optical video microscopy of glassy colloids.[13] Molecular-dynamics studies give insight into this localization process,[14–19] which involves both the translational and the rotational degrees of freedom.[20] The cage concept is rather intuitive and fruitful in that it may be incorporated in formal theoretical treatments of the glassy dynamics, like the mode-coupling theory[21] and recent extensions to deal with polymer chains.[22]

Molecular motion in the presence of cages exhibits different time scales. The fast regime corresponds to the rattling of the trapped particle, the intermediate regime is due to the escape process of this particle, and the slowest regime is ascribed to the cage relaxation with its collective character. Recording experimental data about all these regimes is not trivial and only indirect signatures are often presented.[23]

In the last several years several studies of the cage dynamics by magnetic resonance spectroscopies were reported.[1,24–33]

In particular, multidimensional NMR separates the information about both the geometry and the time scales of the rotational motion of individual polymer groups and provides

[a)]Electronic mail: dino.leporini@df.unipi.it

 © 2003 American Institute of Physics

Downloaded 26 Nov 2003 to 131.114.128.200. Redistribution subject to AIP license or copyright, see http://ojps.aip.org/jcpo/jcpcr.jsp

evidence for memory effects of both aspects.[1] The rotational dynamics of guest molecules in clathrate hydrates was investigated by ^{1}H-NMR by varying both the cage geometries of the host lattice and the properties of the guest species.[24]

Two-dimensional field-step electron–electron double resonance (ELDOR) was used to investigate the reorientation of trapped spin probes and spin labels in glassy polymers.[25–28] The data analysis yielded libration angles in the cages of $2°-10°$ and mean correlation times of a few nanoseconds. Information on both the geometry and the time scales was drawn. The cage motion of both paramagnetic spin probes dissolved in low-molecular-weight liquids and end-labeled polymeric liquid crystals was studied by electron spin resonance (ESR) spectroscopy.[29,30] Cages surrounding the spin labels were found to relax more than two orders of magnitude slower than the local chain-end modes. The orientation relaxation of aligned optically active spin probes in glassy polymeric hosts was also investigated.[32] The probe molecules were found in stochastic fast angular motion in the anisotropic cage of the matrix with average angular displacement which has been estimated as $5°-15°$.

The remarkable orientation resolution of high-field pulsed ESR operating at 95 GHz[34–36] provides a new, complementary way to characterize such motion. A particularly simple situation is encountered at the canonical orientations, where one may expect to obtain simple relations between the parameters of an anisotropic diffusion model and the transverse relaxation time of the electron spins or the time constant for the decay of the stimulated echo. This enables an approach which differs from previous ESR studies in that the reorientation of the spin probes is investigated by analyzing for the same system in the same temperature range the continuous-wave line shape, saturation-recovery, primary and stimulated echoes to cover a wider dynamic range of relaxation times. A preliminary report has been published elsewhere.[33] Notably, primary and stimulated echoes were jointly analyzed before to investigate the optical dephasing of dyes due to the structural relaxation of the glassy host.[7,8]

As a model system to study cage motion over a wide range of time scales we employ ionic spin probes that are immobilized on the surface of ionic clusters in ionomers due to electrostatic attachment.[37,38] Such attachment was found to prevent wide-angle reorientation of the probes up to temperatures that are 100 K higher than the glass transition temperature.[38] Yet, small angle motion at temperatures above the glass transition temperature is expected to depend on rearrangement of the cage surrounding the probe, which is formed by the polymer chains that enter the ionic cluster. This model system thus allows one to study *slow* cage dynamics in a polymer.

The paper is organized as follows: In Sec. II the background on high-field pulsed ESR is presented. The theoretical and numerical tools are discussed in Sec. III. The experimental details are given in Sec. IV. The results are discussed in Sec. V.

II. HIGH-FIELD ESR SPECTROSCOPY

In the system of interest here, the main broadening mechanism of the ESR line shape is the coupling between the reorientation of the spin probe and the relaxation of the electron magnetization via the anisotropy of the Zeeman and the hyperfine magnetic interactions. When the molecule rotates, the coupling gives rise to fluctuating magnetic fields acting on the spin system. The resulting phase shifts and transitions relax the magnetization and broaden the resonance.[39]

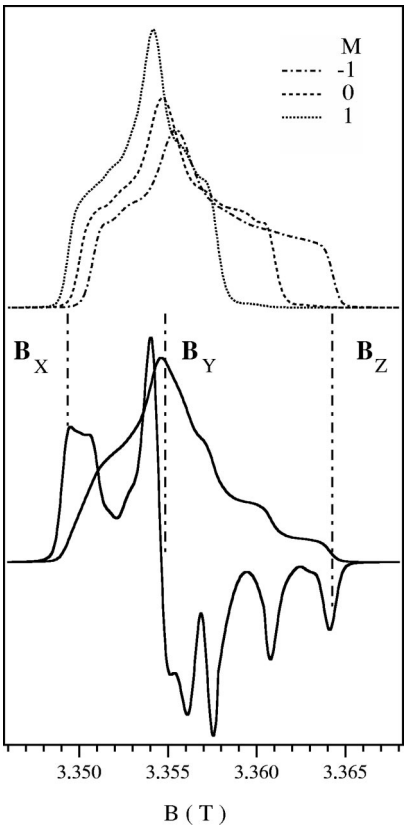

FIG. 1. Structure of the *W*-band ESR line shape of a nitroxide spin probe undergoing very slow reorientation (simulation). Magnetic parameters are listed in Sec. IV. Top: the three hyperfine components. Bottom: the overall absorption (thin line) and the derivative (bold line) line shapes. The spin probe rotates by jumps of size $\theta_0=60°$ with correlation time 46 ns. B_i, $i=x,y,z$ mark the B-field values for selecting spin probes with their x,y,z molecular axes parallel to the static magnetic field, see Fig. 2.

W-band ESR studies on the reorientation of spin probes are carried out at a fixed frequency of about 94 GHz. By sweeping the static field, resonances are found at about 3.5 T. If the spin probes are effectively trapped, the wide-angle reorientation occurs on time scales which may exceed 50 ns so that the cw ESR line shape approaches the rigid-limit pattern. Figure 1 shows a simulation corresponding to this slow dynamical regime based on theory presented elsewhere.[40] In this slow dynamical regime the intensity of the absorption line shape at each B-field value stems from the different resonating contributions due to the spin probes with suitable orientations. The high resolution of the molecular orientations related to each B value by using soft (selective) pulses is a unique feature of high-field ESR.[34,35] In fact, if the spin probe undergoes slow reorientation, the anisotropic Zeeman interaction at high magnetic fields causes a broad dispersion of resonance frequencies, e.g., for nitroxides about 20 mT at *W* band frequencies. This extension of the line shape widely exceeds the excitation band width of

Downloaded 26 Nov 2003 to 131.114.128.200. Redistribution subject to AIP license or copyright, see http://ojps.aip.org/jcpo/jcpcr.jsp

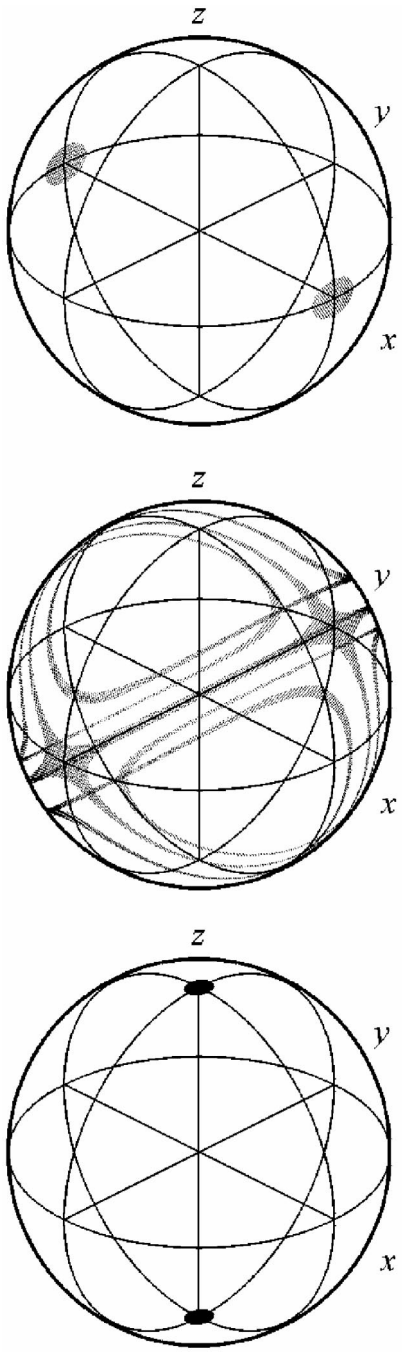

FIG. 2. The selection of orientation subensembles in a *W*-band experiment for the excitation bandwidth of about 0.5 mT and field values B_x (top), B_y (middle), and B_z (bottom). The shaded areas are the orientations of the static magnetic field with respect to the molecular frame of the excited spin probes, see Fig. 1.

the microwave pulses (about 0.5 mT), so that spin probes with well-defined orientations θ_0, ϕ_0 are selected. As an illustration, Fig. 2 shows the subensembles of the overall orientation distribution which are excited by soft pulses if the magnetic field is set at B_i with $i=x,y,z$ (see Fig. 1). They include molecules with their X, Y, and Z molecular axis, i.e., the principal axes of the g and the hyperfine tensors, being aligned with the static magnetic field, respectively. The high-field ESR allows one to characterize the reorientation properties of these subensembles.

To achieve the wide dynamic range which is needed to study the relaxation processes of disordered materials, in addition to cw ESR we jointly used three pulsed experiments detecting the primary electron-spin echo (ESE), the stimulated echo (SE), and the saturation recovery (SR), see also Ref. 36.

The primary ESE experiment is performed with the two-pulse sequence $\pi/2-\tau-\pi-\tau$. By increasing the spacing τ, the amplitude decay of the primary echo $S_{\mathrm{ESE}}(\tau)$ is detected. It vanishes over a typical time scale T_{ESE} [to be defined, e.g., by the time integral of $S_{\mathrm{ESE}}(\tau)/S_{\mathrm{ESE}}(0)$]. For small concentration and hence negligible instantaneous diffusion as in the present study, the time constant of the exponential decay can be identified with the transverse relaxation time, $T_{\mathrm{ESE}}=T_2$. The SE experiment is based on the three-pulse sequence $\pi/2-\tau-\pi/2-T_m-\pi/2-\tau$.[36] The period between the second and the third pulse is usually referred to as the mixing period. It follows the evolution period and precedes the detection period. With increasing mixing-time T_m, the amplitude of the stimulated echo, $S'_{\mathrm{SE}}(T_m)$, decreases. This decay is limited by the longitudinal relaxation of the magnetization which may be corrected for. The decay components remaining after correction are related to changes in the resonance frequency during time T_m. To the slow component of this corrected decay $S_{\mathrm{SE}}(T_m)$ we assign the decay time T_{SE}.

In Sec. V we shall show that the relaxation times of ESE and SE can be rather different, e.g., $T_{\mathrm{SE}}\approx 70T_2$, although both decays are governed by reorientation processes of the spin probe leading to random changes of the resonance frequency (spectral diffusion).

In the ESE experiment two pulses are spaced by a variable temporal interval τ and transverse magnetization is probed. Its dephasing is highly sensitive to reorientation times comparable to $\tau\cong T_{\mathrm{ESE}}$. Faster reorientations average out the dephasing, leading to so-called ''motional narrowing'' and longer T_{ESE}. Slower reorientations are seen as static inhomogeneous broadening to be rephased by the second pulse thus leading to no decay.

The SE experiment may be seen as an extension of the ESE experiment where the second pulse is split in two equal ones to be spaced by the temporal interval T_m, in which information about the spin state is stored as longitudinal magnetization. Then, in addition to the short-time scale τ, a second time scale is probed which is usually at least one order of magnitude longer. The upper limit is set by the spin-lattice relaxation time T_1. Like in the ESE experiment the measured decay rate of the magnetization arises mainly from reorientation times that fall in a certain range. The important difference is that now the range is given by $(\tau,T_m)\cong(\tau,T_{\mathrm{SE}})$ instead of being around τ as in the ESE experiment. Since T_m may be made as long as T_1, the SE experiment is sensitive to slower fluctuations.

In both experiments it is also important to consider that the dynamical processes which are faster than the pulse length t_p are not detected since they do not lead to any echo formation. Then, the actual lower limit of the accessible dynamic range is the longest time between τ and t_p.

In addition to the above-discussed ESE and SE experiments, the spin-lattice relaxation was studied by a saturation-

Downloaded 26 Nov 2003 to 131.114.128.200. Redistribution subject to AIP license or copyright, see http://ojps.aip.org/jcpo/jcpcr.jsp

recovery experiment (SR) by employing a long saturating pulse with two-pulse spin-echo detection.[41–45] The recovery signal is well fitted by a single exponential with decay time T_1. This time T_1 is sensitive to the fast dynamics occurring with rates close to the electron Larmor frequency $\nu_0 = 94$ GHz and thus probes much shorter time scales than ESE and SE ones.

In Sec. III we outline the theoretical and numerical tools that we developed to analyze the ESE and SE decays.

III. THEORETICAL AND NUMERICAL TOOLS

A. ESE spectroscopy

Schwartz *et al.* developed a general theory of electron spin echoes whose numerical results evidenced a square-root dependence of the transverse relaxation time on the diffusion coefficients in the slow-motion regime.[46]

A number of ESR studies pointed out, however, that the angles spanned during the short-time reorientation of the spin probes/labels in the cage are small. Several ELDOR studies set the range $2°-10°$.[25–28] An ESR study estimated $5°-15°$.[32]

In fact, the small-angle assumption proved to be enough to recover the result by Schwartz *et al.* It underlies the theory by Baram for systems with spin $S=1/2$ in the secular approximation,[47] which was extended by Kivelson and Lee[48] to the case of hyperfine interaction to deal with the special case of the parallel edge, i.e., $\theta_0=0$. All these authors assumed isotropic diffusion.

The results by Baram, Kivelson and Lee may be generalized to treat anisotropic diffusion analytically, i.e., without resorting to sophisticated general numerical approaches.[46] Moreover, one notices that close to the canonical orientations of the g and hyperfine tensor (B_i, $i=x,y,z$, see Figs. 1 and 2) the changes in the spin Hamiltonian are small for such small-amplitude motion and, in addition, pseudosecular contributions can be neglected. Thus, the extrema and saddle points of the resonance spectrum can be considered in a simplified treatment in the framework of the anisotropic diffusion model and analytical expressions of the relaxation times $T_{\mathrm{ESE}\,i}=T_{2\,i}$, $i=x,y,z$ can be obtained. The experimental evidence ensuring the consistency of the approach in the present case will be presented in Sec. V C.

Such a model based on small-angle jumps predicts, in agreement with experiment, that the transverse relaxation time is anisotropic, namely it depends on the initial selected orientation θ_0, ϕ_0, $T_2=T_2(\theta_0,\phi_0)$. In contrast, if the reorientation of the spin probe proceeds by large-angle jumps with average rate $1/\tau$, one expects small anisotropy, i.e.,

$$T_{2\,i}\approx\tau, \quad i=x,y,z. \tag{1}$$

In this large-angle regime, T_2 is of the same order of magnitude as the rotational correlation time $\approx\tau$. Instead, in the presence of small-angle jumps, T_2 may be much shorter than the rotational correlation time. This is the regime of interest here.

For a detailed model, we consider molecules with a single $S=1/2$ electron spin and hyperfine interaction with a nucleus having spin I and magnetic quantum number M. The g tensor and the hyperfine tensors are assumed to be diagonal in the same molecular frame with components g_i and A_i, $i=x,y,z$, respectively, a situation resembling that in spin labels.[49,50] The theory could be easily generalized to the case of noncoincident principal axes frames of the two tensors by separately considering the transitions that correspond to different magnetic quantum numbers M of the nuclear spin, since for each value of M, the orientation dependence of the electron spin transition frequency is described by a sum tensor that quantifies the *local* field at the electron spin. Here we let θ and ϕ be the polar and the azimutal angles specifying the direction of the field B in the common principal axis frame of the g and hyperfine tensor. The form of the Hamiltonian $\mathcal{H}$ is[48,51]

$$\mathcal{H}=g(\theta,\phi)\mu_B B S_{z'}+K(\theta,\phi)S_{Z'}I_{Z''}, \tag{2}$$

where μ_B is the Bohr magneton and

$$g(\theta,\phi)=\sqrt{(g_x^2\cos^2\phi+g_y^2\sin^2\phi)\sin^2\theta+g_z^2\cos^2\theta}, \tag{3}$$

$$K(\theta,\phi) = \sqrt{(g_x^2A_x^2\cos^2\phi+g_y^2A_y^2\sin^2\phi)\sin^2\theta+g_z^2A_z^2\cos^2\theta}/\, g(\theta,\phi). \tag{4}$$

The Hamiltonian in Eq. (2) is exact to within second-order terms of order $K^2/g\mu_B B$ which are negligible in the W-band high-field experiment. The electron and the nuclear spins are quantized along axes Z' and Z'', respectively. In general, the axes do not coincide with the direction of the static magnetic field defining the Z axis of the laboratory frame (X,Y,Z) and depend on the orientation of the spin probe.[51] The above-noted Hamiltonian follows from the exact diagonalization of the original form written in the laboratory frame including the secular (S_Z,S_ZI_Z), the pseudosecular $(S_Z,S_ZI_{X,Y})$, and the nonsecular $S_{X,Y}$ terms. If very slow reorientation processes are considered, the nonsecular terms may be dropped. This sets $Z'=Z$. We will also set $Z''=Z$. This follows since we evaluate the relaxation following the selective excitation at the canonical orientations B_i, $i=x,y,z$ where the resonating spin probes are oriented with one of their principal axes parallel to B (see Figs. 1 and 2). In this configuration the axes Z'' and Z coincide.[51] It will be shown later that, during the relaxation times T_2 and T_{SE}, the spin probes span only small angular ranges ensuring that the equality $Z''=Z$ fairly holds in the whole time window of interest. In fact, it may be shown that letting $Z''=Z$ corresponds to partial neglect of the pseudosecular terms. The approximation works nicely even in the less favorable X-band case if excitation is selective at B_i, $i=x,y,z$.[48] On this basis we rewrite the Hamiltonian Eq. (2) as

$$\mathcal{H}=\sum_{M=-I}^{I}\omega_M(\theta,\phi)P_M S_Z. \tag{5}$$

P_M is the projector on the I-spin subspace with magnetic quantum number M in the laboratory frame and

$$\omega_M(\theta,\phi)=g(\theta,\phi)\mu_B B+K(\theta,\phi)M. \tag{6}$$

Downloaded 26 Nov 2003 to 131.114.128.200. Redistribution subject to AIP license or copyright, see http://ojps.aip.org/jcpo/jcpcr.jsp

The density matrix describing the spin system after the first excitation pulse is written as

$$\rho=\sum_{M=-I}^{I}\rho_M(\Omega,t)P_M S_+, \tag{7}$$

where S_+ is the rising operator in the laboratory frame. $\rho_M(\Omega,t)$ depends on the orientation Ω at time t and fullfills the stochastic Liouville equation[52]

$$\frac{d}{dt}\rho_M(\Omega,t)=(-i\omega_M(\Omega)+\Gamma)\rho_M(\Omega,t). \tag{8}$$

The operator Γ describes the reorientation process and reads[52]

$$\Gamma=-[D_\perp L^2+(D_\parallel-D_\perp)L_z^2]. \tag{9}$$

L^2 and L_z are the modulus and the z axis projection of the angular momentum, respectively. $D_\parallel$ and $D_\perp$ are the components of the diffusion tensor for the small-angle motion.

To derive the analytical expressions of $T_2(\theta_0,\phi_0)$, Eq. (8) will be solved with the initial conditions $\theta(0)=\theta_0$ and $\phi(0)=\phi_0$. The underlying assumption is that all the spins excited by the first $\pi/2$ pulse of the ESE sequence are refocused by the second one. In principle, part of the initially excited magnetization could be lost due to the spectral diffusion and the small excitation bandwidth of the second pulse. Our choice of exciting at $B_{x,y,z}$, however, corresponds to the extrema or the saddle points of the resonance frequencies $\omega_M(\theta,\phi)$ of the M hyperfine components where the spectral diffusion is at a minimum (Fig. 1). Indeed, it will be shown in Sec. V C that magnetization loss at these orientations is negligible.

For brevity, the dependence on M will be dropped henceforth. Furthermore, $\omega_M(\theta,\phi)$ will be denoted as $\omega_x(\theta_0=\pi/2,\phi_0=0)$, $\omega_y(\theta_0=\pi/2,\phi_0=\pi/2)$, and $\omega_z(\theta_0=0)$. With no loss of generality, we may assign the two extrema at ω_y, ω_z and the saddle point to ω_x, respectively, i.e., $|\omega_y-\omega_0|<|\omega_x-\omega_0|<|\omega_z-\omega_0|$.

Owing to the small angular range spanned during T_2, the resonance frequencies are shifted only by small amounts between the first and the second pulse. The offsets with respect to ω_i $i=x,y,z$ are then expressed as

$$\delta\omega_x=-\frac{\eta_x-3}{2}f_{0\,x}\delta\theta^2-\eta_x f_{0\,x}\delta\phi^2, \tag{10}$$

$$\delta\omega_y=\frac{\eta_y+3}{2}f_{0\,y}\delta\theta^2+\eta_y f_{0\,y}\delta\phi^2, \tag{11}$$

$$\delta\omega_z=\frac{\eta_z\cos 2\phi-3}{2}f_{0\,z}\delta\theta^2, \tag{12}$$

where $\delta\theta=\theta-\theta_0$ and $\delta\phi=\phi-\phi_0$. The explicit expressions of η_i and f_{0i} are listed in Appendix A. If $\eta_x=\eta_y=\eta_z=\eta$ and $f_{0x}=f_{0x}=f_{0x}=f_0$, Eqs. (10)–(12) correspond to the ones of a fictitious $S=1/2$ spin in the presence of a secular Zeeman interaction with asymmetry parameter η and strength f_0.[47]

We are now in a position to derive the expressions of the transverse relaxation times T_{2i} after the excitation at B_i, $i=x,y,z$ by solving Eq. (8). The equation may be recast in the form of the Schrödinger equation of the harmonic oscillator, as was noted by Baram for the simple case of a system with $S=1/2$ in the secular approximation.[47] In Appendix B it is extended to the present case. This provides the following expressions:

$$T_{2\,x}^{-1}=\frac{\sqrt{f_{0\,x}}}{2}\{\sqrt{(3-\eta_x)D_\perp}+\sqrt{2\eta_x D_\parallel}\}, \tag{13}$$

$$T_{2\,y}^{-1}=\frac{\sqrt{f_{0\,y}}}{2}\{\sqrt{(3+\eta_y)D_\perp}+\sqrt{2\eta_y D_\parallel}\}, \tag{14}$$

$$T_{2\,z}^{-1}=\frac{\sqrt{f_{0\,z}}}{2}\{\sqrt{3-\eta_z}+\sqrt{3+\eta_z}\}\sqrt{D_\perp}. \tag{15}$$

We stress again that the above-presented model can only be applied if the angular range spanned during T_2 is small, i.e.,

$$DT_2\ll 1. \tag{16}$$

DT_2 is the largest product to be obtained by combining the diffusion coefficients $D_\parallel$ and $D_\perp$ with the transverse relaxation times T_{2x}, T_{2y}, and T_{2z}. The above-noted inequality states that the rotational correlation time is much longer than T_2.

B. SE spectroscopy

Mims and co-workers investigated how the stimulated echo is affected by spectral diffusion, but the case when the latter is due to the molecular reorientation was not addressed.[53–55] Poor attention has been paid to that issue in ESR spectroscopy. In fact, in spite of large efforts in multidimensional solid-state NMR to clarify the influence of the molecular reorientation on SE[1] (see also Refs. 56 and 57 for related 1D-NMR studies), we are not aware of similar investigations for the ESR case. Extending the NMR analysis to ESR spectroscopy is not straightforward due to the rather different excitation bandwidths and the one-dimensional character of the ESR-SE spectroscopy.

As the mixing time T_m can be much longer than T_2, the SE decay can take place on a time scale which is more than one order of magnitude longer than the ESE time scale. We evaluate this decay according to a Monte Carlo scheme under fairly general assumptions.

Here we focus on the role played by the spectral diffusion in the mixing period and neglect, as usual, any related effect during the evolution and the detection periods which are more than one order of magnitude shorter.[53–55] In this case the longitudinal magnetization after the second pulse exhibits a grated pattern if it is plotted in terms of the offset between the microwave ω and the Larmor angular frequencies, $\Delta\omega=\omega_0-\omega$.[53,54] The relevant terms contributing to the SE echo are proportional to $\cos(\Delta\omega\tau)$ and $\sin(\Delta\omega\tau)$ and will be referred to as $G'(\Delta\omega)$ (see Fig. 3). The width of the pattern is set by the excitation bandwidth of the pulses, which is much smaller than the inhomogeneous total width of the broadened ESR line. The periodicity of the pattern is approximately given by $2\pi/\tau+t_p$, with t_p being the pulse length.[55] If the excitation bandwith is much larger than the inhomogeneous linewidth the periodicity is $2\pi/\tau$.

Downloaded 26 Nov 2003 to 131.114.128.200. Redistribution subject to AIP license or copyright, see http://ojps.aip.org/jcpo/jcpcr.jsp

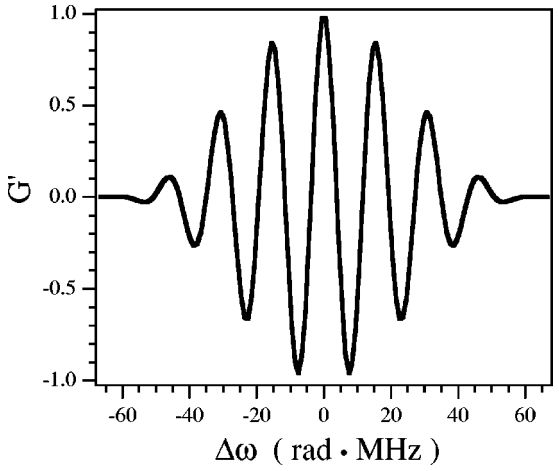

FIG. 3. The grated pattern G' in the SE experiment. The length of the pulses is $t_p=100$ ns, $\tau=3t_p$. The Rabi frequency $\omega_1=8.7$ rad MHz. See the text for details.

During the mixing period, spectral diffusion changes the resonance frequencies of the excited spin packets, thus blurring the grated pattern. At the end of the mixing period it has the new shape $G'(\Delta\omega,T_m)$ $(G'(\Delta\omega,0)\equiv G'(\Delta\omega))$. The third pulse rephases the spin packets and at the end of the detection period the stimulated echo is formed. If spectral diffusion in the detection period is negligible, the stimulated echo may be expressed as

$$S_{\mathrm{SE}}(T_m)=\left\langle \int d\Delta\omega G'(\Delta\omega,T_m)G''(\Delta\omega)\right\rangle. \tag{17}$$

$G''(\Delta\omega)$ accounts for the rephasing after the third pulse. It may be expressed in analytic form and is very similar to $G'(\Delta\omega)$. The integral collects the contributions of all the spin packets and the angular brackets denote a suitable average over all the random reorientation paths during the mixing period.

Equation (17) is interesting in that it expresses the SE signal as the cross-correlation function of G' and G''. It is a general expression provided that the spectral diffusion in the evolution and the detection periods can be neglected. In particular, in the limit of large excitation bandwidth $G'(x)=G''(x)=\cos(x)$ and well-known results from NMR are recovered.[1]

Thus, Eq. (17) extends Mims' derivation of the SE decay in the limit of large excitation bandwidth and negligible spectral diffusion during the evolution and the detection periods.[54,55] We note that

$$G'(\Delta\omega,T_m)=\int d\Delta\omega_i K_D(\Delta\omega-\Delta\omega_i,T_m)G'(\Delta\omega_i). \tag{18}$$

In Mims' notation K_D is the diffusion kernel describing the spectral diffusion of one spin packet from the initial resonance frequency $\Delta\omega_i$ to $\Delta\omega$. In the limit of large excitation bandwidth Eq. (17) recovers Mims' result that $S_{\mathrm{SE}}(T_m)$ is the cosine Fourier transform of $K_D(\omega,T_m)$.[54,55]

The calculation of $S_{\mathrm{SE}}(T_m)$ by Eq. (17) has been carried out by numerical methods. To this aim a suitable model of the spectral diffusion by molecular reorientation is needed. The time evolution of two angles is of interest, namely the evolution of the second and third Euler angles, θ and ϕ, which together with the first one (of no relevance in isotropic hosts) describe the rotation from the laboratory axis (Z axis along with the static magnetic field) to the molecular axis.[58] We assume that θ and ϕ undergo random jumps. To limit the adjustable parameters, the dynamics of θ is taken to be independent of ϕ, i.e., the reorientation is cylindrically symmetric around the z molecular axis. The distribution of the jump sizes is flat with zero average and root mean squared values $\Delta\theta$ and $\Delta\phi$. Alternative distributions, e.g., one single jump size, resulted in slightly worse fits of our experimental data with equal number of adjustable parameters. We assume Poisson statistics for the distribution of the waiting times between jumps, i.e., an exponential distribution with mean waiting times τ_θ and τ_ϕ.[59] At long times, θ and ϕ are Gaussian variables with rotational diffusion coefficients $D_\perp$ and $D_\parallel$, respectively,

$$D_\parallel=\frac{\Delta\phi^2}{2\tau_\phi}, \tag{19}$$

$$D_\perp=\frac{\Delta\theta^2}{4\tau_\theta}. \tag{20}$$

If the jump size is sufficiently small the above-noted model reduces to the rotational diffusion model and $D_\parallel$ and $D_\perp$ set the rotational correlation times.[60] Larger jumps cause correlation loss before the onset of the diffusive regime.

The above-mentioned dynamics leads to the spectral diffusion via Eq. (6) and was used to evaluate $S_{\mathrm{SE}}(T_m)$ via Eq. (17) by Monte Carlo (MC) methods. For typical excitation bandwidth, pulse length and τ spacing of the SE experiment at W-band frequencies as well as standard magnetic parameters of nitroxides the decay is virtually exponential with decay time $\mathcal{T}_{\mathrm{SE}}$, yet anisotropic. Figure 4 shows typical results for the SE decays at B_i with $i=x,y,z$, the related decay times will be denoted to as $\mathcal{T}_{\mathrm{SE}\,i}$, $i=x,y,z$. Extensive results about them are listed in Table I to illustrate the general features of the model.

If the decay is caused by θ fluctuations only (entries 1–4 of Table I), the anisotropy is weak and the MC results are well approximated by

$$\tilde{\mathcal{T}}_{\mathrm{SE}\,i}|_{\Delta\phi=0}=\tau_\theta, \quad i=x,y,z. \tag{21}$$

Equation (21) means that, even a single, small θ jump cancels the correlation between the grating functions $G'(\Delta\omega,T_m)$ and $G''(\Delta\omega)$ [Eq. (17)]. The decay is just proportional to the distribution of the waiting times, before a new θ jump takes place, $\psi_\theta(t)$. If the decay is caused by ϕ fluctuations only (entries 5–8 of Table I), for large $\Delta\phi$ values the MC results are well approximated by

$$\tilde{\mathcal{T}}_{\mathrm{SE}\,i}|_{\Delta\theta=0}=\tau_\phi, \quad i=x,y,z. \tag{22}$$

In this limit the SE decay yields the waiting-time distribution before a new jump of ϕ takes place, $\psi_\phi(t)$. For *smaller* $\Delta\phi$, $\mathcal{T}_{\mathrm{SE}\,x,y}$ are still well fitted by Eq. (22) and the SE decays at B_x and B_y still correspond to $\psi_\phi(t)$. However, the anisotropy of the relaxation times is much larger and Eq. (22) fails for $\mathcal{T}_{\mathrm{SE}\,z}$. This is understood by inspecting the dependence of

Downloaded 26 Nov 2003 to 131.114.128.200. Redistribution subject to AIP license or copyright, see http://ojps.aip.org/jcpo/jcpcr.jsp

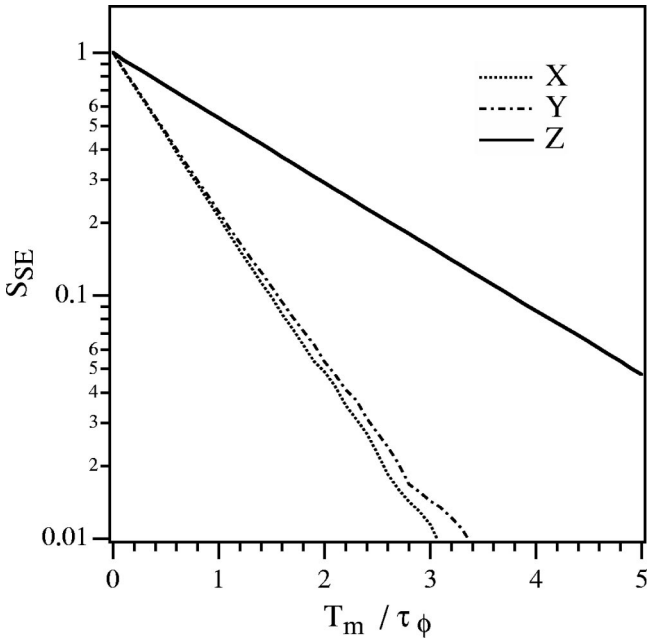

FIG. 4. Typical decays of the stimulated echo $S_{SE}(T_m)$ excited at B_x, B_y, and B_z (Monte Carlo simulation). $\Delta\theta = 34.4°$, $\Delta\phi = 2.9°$, $\tau_\theta/\tau_\phi = 2$. Pulse-sequence parameters as in Fig. 3. Magnetic parameters are listed in Sec. IV.

the resonance magnetic field on θ and ϕ, $\omega_M(\theta,\phi)/\gamma$ [Eq. (6)]. Around B_z, *small* changes in the ϕ angle do not displace the resonance field appreciably and then a diffusive ϕ dynamics does not contribute to the decay. It is worth noting that the analogous effect does not occur for the θ angle.

The general case $\Delta\theta$, $\Delta\phi \neq 0$ is also presented in Table I (entries 9–21). Several regimes are covered:

(i) small $\Delta\phi$ values (entries 9–11),
(ii) intermediate $\Delta\phi$ values, $\Delta\theta/\Delta\phi < 1$ and arbitrary ratio τ_θ/τ_ϕ (entries 12–14),
(iii) intermediate $\Delta\phi$ values, arbitrary ratio $\Delta\theta/\Delta\phi$ and $\tau_\theta/\tau_\phi > 1$ (entries 14–17),
(iv) large $\Delta\phi$ values (entries 19–21),
(v) $\tau_\theta < \tau_\phi$ (entries 12 and 18).

For use in easy and approximate data analysis, the MC results, which were obtained without making any specific assumptions on the relation between the dynamic process and the relaxation times, are compared with the following approximation:

$$\frac{1}{\tilde{\mathcal{T}}_{\mathrm{SE}\ i}} = \frac{1}{\mathcal{T}_{\mathrm{SE}\ i}}\bigg|_{\Delta\theta=0} + \frac{1}{\tau_\theta}, \quad i = x,y,z. \tag{23}$$

Equation (23) is a guess motivated by the independence of θ and ϕ dynamics and the above-presented discussion of the MC results. It works effectively in the range of interest. A simplified version of Eq. (23) is achieved by approximating the $\mathcal{T}_{\mathrm{SE}\ i}$ by Eq. (22):

$$\frac{1}{\tilde{\mathcal{T}}_{\mathrm{SE}\ i}} = \frac{1}{\tau_\phi} + \frac{1}{\tau_\theta}, \quad i = x,y,z. \tag{24}$$

The above-given expression is expected to account for dynamical regimes with small anisotropy of the relaxation times. In the case of stronger anisotropy (small $\Delta\phi$ values) $\mathcal{T}_{\mathrm{SE}\ z}|_{\Delta\theta=0} \gg \tau_\theta$ and, since $\mathcal{T}_{\mathrm{SE}\ x,y}|_{\Delta\theta=0} \approx \tau_\phi$, Eq. (23) approaches the limiting form

$$\frac{1}{\tilde{\mathcal{T}}_{\mathrm{SE}\ x,y}} = \frac{1}{\tau_\phi} + \frac{1}{\tau_\theta}, \tag{25}$$

TABLE I. Monte Carlo results on $\mathcal{T}_{\mathrm{SE}\ i}$, $i = x,y,z$. The columns $\tilde{\mathcal{T}}_{\mathrm{SE}\ i}$ are the corresponding approximations as given by Eqs. (21), (22), and (23). Magnetic parameters as listed in Sec. IV. Excitation bandwidth, pulse length, and τ spacing as in Fig. 3. Any time is in units of Monte Carlo steps.

	$\Delta\phi$(deg)	$\Delta\theta$(deg)	τ_ϕ	τ_θ	$\mathcal{T}_{\mathrm{SE}\ x}$	$\mathcal{T}_{\mathrm{SE}\ y}$	$\mathcal{T}_{\mathrm{SE}\ z}$	$\tilde{\mathcal{T}}_{\mathrm{SE}\ x}$	$\tilde{\mathcal{T}}_{\mathrm{SE}\ y}$	$\tilde{\mathcal{T}}_{\mathrm{SE}\ z}$	Equation
1	0	2.9	⋯	10	10.8	9.97	9.64	10	10	10	(21)
2	0	5.7	⋯	10	9.9	9.8	9.7	10	10	10	(21)
3	0	11.5	⋯	10	9.8	9.7	9.7	10	10	10	(21)
4	0	34.4	⋯	10	9.7	9.8	9.7	10	10	10	(21)
5	2.9	0	10	⋯	9.51	11.5	99.8	10	10	10	(22)
6	6.9	0	10	⋯	9.1	9.9	23.7	10	10	10	(22)
7	11.5	0	10	⋯	9.4	10	13.7	10	10	10	(22)
8	34.4	0	10	⋯	9.4	9.7	11.6	10	10	10	(22)
9	2.9	34.4	10	10	4.75	5.0	8.70	4.87	5.34	9.08	(23)
10	2.9	34.4	10	20	6.60	7.20	16.4	6.44	7.30	16.6	(23)
11	2.9	34.4	10	40	7.61	8.98	28.5	7.68	8.93	28.5	(23)
12	6.9	2.9	10	2.5	2.0	2.0	2.14	2.0	2.0	2.26	(23)
13	6.9	2.9	10	5	3.7	3.1	3.79	3.2	3.3	4.1	(23)
14	6.9	2.9	10	20	6.25	6.62	10.72	6.25	6.62	10.8	(23)
15	6.9	22.9	10	20	6.10	6.45	10.65	6.25	6.62	10.8	(23)
16	6.9	34.4	10	20	6.11	6.53	10.67	6.25	6.62	10.8	(23)
17	6.9	90	10	20	6.10	6.49	10.87	6.25	6.62	10.8	(23)
18	6.9	90	10	2.5	2.0	2.0	2.20	1.96	1.99	2.26	(23)
19	11.5	34.4	10	20	6.30	6.45	7.72	6.39	6.66	8.12	(23)
20	34.4	34.4	10	20	6.32	6.41	6.92	6.37	6.53	7.34	(23)
21	90	34.4	10	20	6.32	6.40	6.71	6.37	6.50	6.95	(23)

Downloaded 26 Nov 2003 to 131.114.128.200. Redistribution subject to AIP license or copyright, see http://ojps.aip.org/jcpo/jcpcr.jsp

TABLE II. Comparison between selected Monte Carlo results on $\mathcal{T}_{\mathrm{SE}\,i}$, $i=x,y,z$ from Table I and the corresponding approximations $\tilde{\mathcal{T}}_{\mathrm{SE}\,i}$ as given by Eqs. (24) and (25).

	$\Delta\phi$(deg)	$\Delta\theta$(deg)	τ_ϕ	τ_θ	$\mathcal{T}_{\mathrm{SE}\,x}$	$\mathcal{T}_{\mathrm{SE}\,y}$	$\mathcal{T}_{\mathrm{SE}\,z}$	$\tilde{\mathcal{T}}_{\mathrm{SE}\,x}$	$\tilde{\mathcal{T}}_{\mathrm{SE}\,y}$	$\tilde{\mathcal{T}}_{\mathrm{SE}\,z}$	Equation
1	2.9	34.4	10	10	4.75	5.0	8.70	5	5	5	(24)
								5	5	10	(25)
2	2.9	34.4	10	20	6.60	7.20	16.4	6.67	6.67	6.67	(24)
								6.67	6.67	20	(25)
3	2.9	34.4	10	40	7.61	8.98	28.5	8.0	8.0	8.0	(24)
								8.0	8.0	40	(25)
4	6.9	2.9	10	2.5	2.0	2.0	2.14	2.0	2.0	2.0	(24)
								2.0	2.0	2.5	(25)
5	6.9	2.9	10	5	3.7	3.1	3.79	3.3	3.3	3.3	(24)
								3.3	3.3	5.0	(25)
6	6.9	2.9	10	20	6.25	6.62	10.72	6.7	6.7	6.7	(24)
								6.7	6.7	20.0	(25)
7	6.9	22.9	10	20	6.10	6.45	10.65	6.7	6.7	6.7	(24)
								6.7	6.7	20.0	(25)
8	6.9	34.4	10	20	6.11	6.53	10.67	6.7	6.7	6.7	(24)
								6.7	6.7	20.0	(25)
9	6.9	90	10	20	6.10	6.49	10.87	6.7	6.7	6.7	(24)
								6.7	6.7	20.0	(25)
10	6.9	90	10	2.5	2.0	2.0	2.20	2	2	2	(24)
								2	2	2.5	(25)
11	11.5	34.4	10	20	6.30	6.45	7.72	6.7	6.7	6.7	(24)
								6.7	6.7	20.0	(25)
12	34.4	34.4	10	20	6.32	6.41	6.92	6.7	6.7	6.7	(24)
								6.7	6.7	20.0	(25)
13	90	34.4	10	20	6.32	6.40	6.71	6.7	6.7	6.7	(24)
								6.7	6.7	20.0	(25)

$$\frac{1}{\tilde{\mathcal{T}}_{\mathrm{SE}\,z}}=\frac{1}{\tau_\theta}.$$

Table II compares Eqs. (24) and (25) with the relevant MC results from Table I. It is seen that they provide rather good approximations for $\mathcal{T}_{\mathrm{SE}\,x,y}$ and upper and lower bounds to $\mathcal{T}_{\mathrm{SE}\,z}$.

The above-noted model of the SE decay predicts the anisotropy of the relaxation times if the reorientation around the z molecular axis is diffusive and is faster than the reorientation of the axis itself. One assumption of the model is that the correlations between θ and ϕ jumps are neglected. If the correlations were not negligible, θ and ϕ should change on similar time scales. This enhances the influence of θ on the SE decay and, consequently, reduces the anisotropy of the decay times, as may be anticipated by Eq. (23).

IV. EXPERIMENT

End-capped poly(isoprene) homopolymer (PI-S10) was prepared by anionic polymerization and subsequent introduction of the ionic end groups as described elsewhere.[37,38] The molecular characteristics of the end-functionalized poly(isoprene) ionomer, denoted as PI-S10, are listed in Table III together with the glass-transition temperature. The schematic representation of PI-S10 is shown in Fig. 5 emphasizing the mesoscopic structure. The sulfonate ionic parts segregate and form nanoscale clusters (multiplets) whose dynamics is severely limited by the poly(isoprene) chains.[61,62] The sample characterization has been described elsewhere.[37] In particular, the studies proved that the multiplet size in PI-S10 is about 1.9 nm.[63]

The free radicals used as spin probes were neutral TEMPO and the potassium salt of 4-carboxy-TEMPO (K-TEMPO, Fig. 5). TEMPO was purchased from Aldrich. The spin probe 4-carboxy-TEMPO (Aldrich) was converted to its potassium salt (K-TEMPO) by titration with 0.1 mM methanolic KOH. Both radicals have one unpaired electron spin $S=1/2$ subject to hyperfine interaction with the nitrogen nucleus with spin $I=1$. The samples for ESR studies were prepared by solvent casting: 100 mg of the polymer was dissolved in 10 mL of toluene and mixed with the calculated amount of 0.05% methanolic spin probe solution such that the ratio of spin probes per ionic chain ends was 2/15. This ensures the presence of two spin probes per each ionic cluster on average.[63] To favor the mixing of K-TEMPO and ionomers, 50 μL of ethanol was added. After film casting and solvent evaporation the samples were dried and annealed under vacuum at 60 °C for about 6 h, before being transferred to the ESR tube. The magnetic parameters of

TABLE III. Molecular characteristics and glass-transition temperature of the PI-S10 ionomer.

M_n (kg/mol)	10
M_w/M_n	1.07
1,4-PI (mol %)	19
T_g(PI) (K)	281

Downloaded 26 Nov 2003 to 131.114.128.200. Redistribution subject to AIP license or copyright, see http://ojps.aip.org/jcpo/jcpcr.jsp

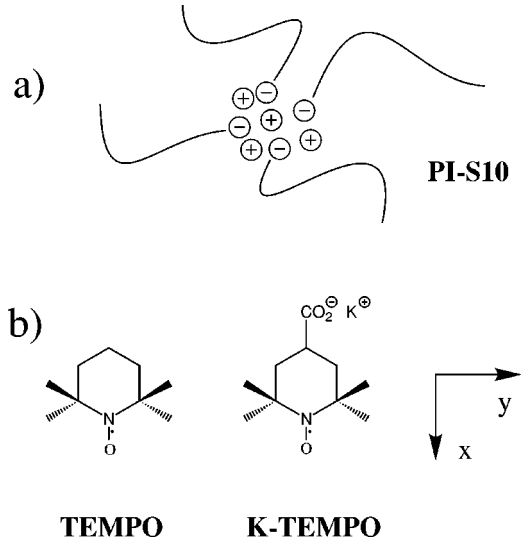

FIG. 5. Schematic representation of the investigated ionomer (a) and the chemical structures of the spin probes (b). Note the segregation into clusters (multiplets) of the ionic part of the polymeric chain and the counterions. The principal magnetic frame of the spin probes is also shown. The x axis is parallel to the N–O bond, the z axis is parallel to the nitrogen and oxygen $2p$ orbitals containing the unpaired electron, and the y axis is perpendicular to the paper plane.

K-TEMPO were measured at low temperature by fitting the ESR line shape. The best fit values are $g_x=2.0095$, $g_y=2.0064$, $g_z=2.0021$, $A_x=18.5$ MHz, $A_y=18.5$ MHz, $A_z=95$ MHz. Both cw and pulsed ESR experiments were carried out on a Bruker E680 spectrometer working at 94 GHz (W band) with the Bruker Teraflex probehead. The length of a $\pi/2$ pulse is about 180 ns. The pump pulse of the SR experiment was 40 μs long. Longer pulses did not change the SR signal proving that the relaxation components due to the spectral diffusion and T_{1n} processes were effectively suppressed. In fact, in the slow-motion regime T_{1n} is at least one order of magnitude shorter than T_1.[42,64] A double-exponential fit of the SR signal was used to eliminate the decay due to the longitudinal spin-relaxation from the SE signal. The pulse sequences for ESE, SE, and SR experiments were suitably phase-cycled to remove spurious decays. Variable-temperature measurements with liquid nitrogen cooling were performed using an Oxford CF935 cryostat and ITC502 temperature control unit.

V. RESULTS AND DISCUSSION

Here we present the characterization of the reorientation of the spin probes in PI-S10. As noted earlier, both cw and pulsed techniques were used to achieve a wide dynamic range.

A. Continuous-wave ESR: Spin-probe location

The first characterization of the reorientation process of the spin probes was provided by cw ESR. The line shapes of TEMPO and K-TEMPO in PI-S10 at T_g+14 K (295 K) are shown in Fig. 6. The TEMPO line shape exhibits marked motional narrowing which indicates large-angle, fast reorientation. Numerical simulation of the line shape carried out by the theory presented in Ref. 40 yields a rotational correlation

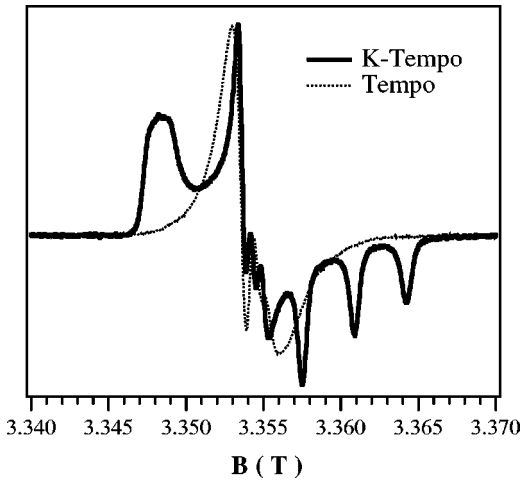

FIG. 6. cw ESR line shapes of TEMPO and K-TEMPO in PI-S10 at 295 K. Note the extensive motional narrowing of the TEMPO line shape.

time $\tau\approx 2$ ns. On the other hand, the K-TEMPO line shape exhibits the rigid-limit pattern at T_g+14 K. This feature extends over a wide temperature range from T_g-101 K, the lowest temperature studied, up to T_g+40 K (Fig. 7) and sets boundaries on the motion of K-TEMPO. Large-angle reorientation, if any, occurs with correlation time $\tau\gg 50$ ns (see Fig. 1). Faster reorientation may occur but must then be restricted to a limited angular range as no appreciable motional narrowing is manifest in the line shape. A rough estimate of the size is given by the broadening of the edges at B_x and B_z (see Fig. 1).[48] At 295 K these are about 0.2 and 0.4 mT, respectively, leading to the result that the changes of the ϕ and θ angles cannot have sizes larger than $\phi_0\cong\theta_0\cong 10°$.

At T_g+40 K the structural relaxation time of PI-S10 is $\tau_\alpha\approx 1\,\mu$s, as estimated by the "universal" Williams–Landel–Ferry (WLF) law for linear amorphous polymers.[65] This evidences the higher decoupling between TEMPO and the polymer structural relaxation with respect to K-TEMPO. Due to the similar molecular shape and size of the spin probes, the immobilization of K-TEMPO is ascribed to the effective attachment to the ionic clusters of the ionomers, as was concluded by earlier cw ESR studies at X band (9.4

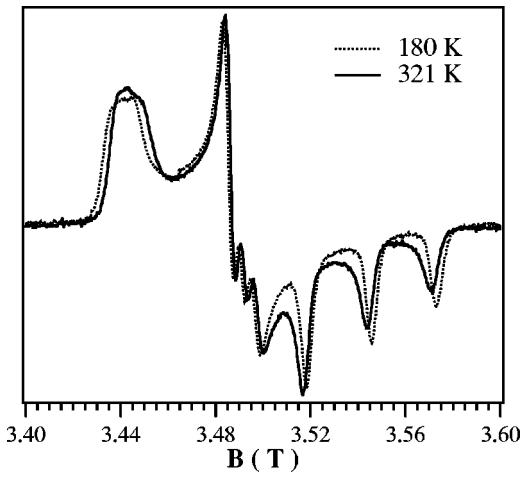

FIG. 7. cw ESR line shape of K-TEMPO in PI-S10 at 180 and 321 K.

Downloaded 26 Nov 2003 to 131.114.128.200. Redistribution subject to AIP license or copyright, see http://ojps.aip.org/jcpo/jcpcr.jsp

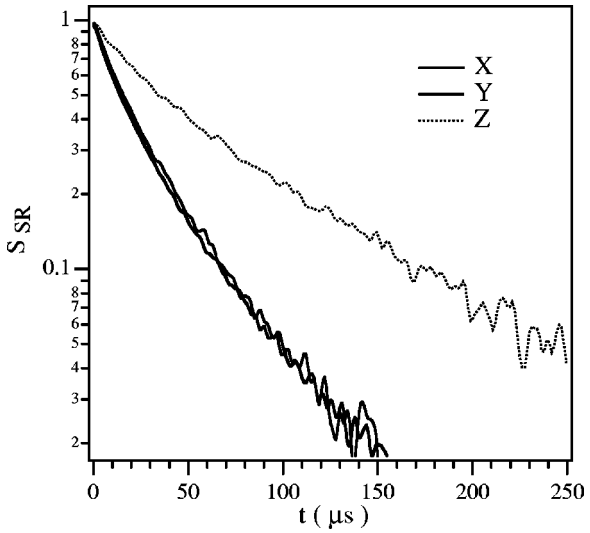

FIG. 8. The decay of the SR signal of K-TEMPO in PI-S10 at B_x, B_y, and B_z, $T=180$ K. Time t is the waiting time between the long saturating pulse and the two-pulse spin-echo detection.

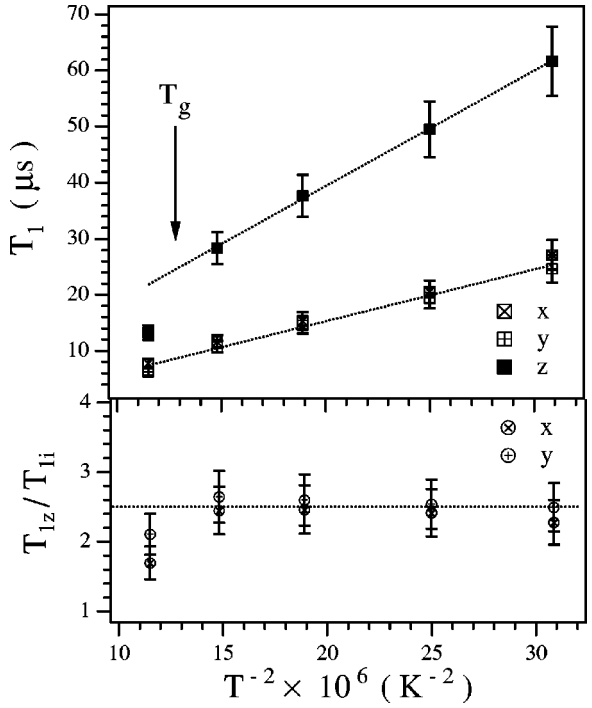

FIG. 9. The temperature dependence of the spin-lattice relaxation times measured at B_x, B_y, and B_z (top) and their ratio (bottom). The dotted lines are the best-fit results according to a squared-temperature dependence. Note the change of regime above T_g for T_{1z} but not for $T_{1x,y}$.

GHz) on K-TEMPO in PI-S10.[38] In particular, they investigated the so-called T_{50G}, the temperature where the spin probe has correlation time $\tau \approx 10$ ns.[66] For K-TEMPO in PI-S10 $T_{50G}=T_g+100$ K was found, where $\tau_\alpha \approx 1$ ns according to the universal WLF law. This is consistent with our observation that the slow reorientation of K-TEMPO at T_g+40 K yields a negligible motional narrowing of the *W*-band line shape.

B. Saturation recovery: Local vibrations, librations, and the cage opening

Figure 8 shows typical decay curves, $S_{\mathrm{SR}}(t)$, describing the recovery of the longitudinal magnetization to the equilibrium value, i.e., $M_z(t) \propto M_{z\infty} - S_{\mathrm{SR}}(t)$. Here, t is the waiting time between the long saturating pulse and the two-pulse spin-echo detection. The decays are almost exponential with decay times T_1. Notice the virtual coincidence of $S_{\mathrm{SR}\,x}$ and $S_{\mathrm{SR}\,y}$.

The spin-lattice relaxation time T_1 is set by processes allowing for transitions between the two electron spin states. For organic free radicals dissolved in solid and glassy hosts different contributions were identified.[67] Studies at *S*, *X*, and *W* bands of nitroxides were recently reported.[43–45] Above the Debye temperature ($\approx 50-100$ K) it was found that the spin-lattice relaxation time is set by two processes: an activated process, being assigned to the nitroxyl ring methyl group rotation, and a second-order Raman process.[51] The latter dominates at *W* band and is responsible for the temperature dependence $T_1 \propto T^{-2}$. The role of intramolecular vibrations in causing the anisotropy of T_1 was anticipated also by ELDOR studies.[28]

As shown in Fig. 9 the spin-lattice relaxation time of K-TEMPO exhibits a temperature dependence which is consistent with a square law up to T_g. However, the investigated range is too limited to assess the temperature dependence unambiguously. The spin-lattice relaxation is anisotropic. It exhibits clear uniaxial features with a ratio $T_{1z}/T_{1x,y}$ about 2.5 (Figs. 8 and 9) in agreement with previous studies on nitroxides-doped single-crystals.[43,45]

In fact, both the magnitude and the temperature dependence of T_1 of K-TEMPO parallel the ones of TEMPOL in organic single crystals.[43,45] T_{1x} of K-TEMPO is 27 and 12 μs at 180 and 260 K, respectively, whereas at the same temperatures T_1 of TEMPOL in an organic single crystal is 39 and 18 μs in the perpendicular region of the ESR spectrum.[45] This supports the conclusion of Refs. 43 and 45 that the molecular vibrations relaxing the longitudinal magnetization of the radical via the Raman process have local character in solid hosts.

The description of the localized vibrations in terms of harmonic modes leads to a temperature dependence $T_1 \propto T^{-2}$ at high temperatures irrespective of the details of the spin-vibration coupling.[68] The localized modes are believed to couple to the spin system via the spin–orbit coupling modulating the g anisotropy.[43] Further consideration of both the anisotropy in the vibrations of the C_2NO unit of the nitroxide moiety and the impact of the vibrations on the g values provided arguments to quantify the ratio $T_{1z}/T_{1x,y}$.[43]

Figure 9 shows that the low-temperature regime extends up to T_g+14 K for $T_{1x,y}$ but T_{1z} deviates due to a larger decrease. K-TEMPO exhibits the same behavior in other ionomers, too.[69]

At temperatures higher than the glass transition temperature T_g, the cage surrounding the spin probe softens and large-scale cooperative motions unfreeze. The increased free volume is expected to enhance the amplitude and, possibly, to change the rate of the small-angle librations of K-TEMPO

Downloaded 26 Nov 2003 to 131.114.128.200. Redistribution subject to AIP license or copyright, see http://ojps.aip.org/jcpo/jcpcr.jsp

in the cage in close analogy with the behavior of local relaxation of polymeric and low-molar mass glasses.[70] This opens up a further path for spin-lattice relaxation. Let us estimate the contribution to $1/T_1$. At *W*-band frequencies the Zeeman interaction is the most important interaction due to the large modulation of its anisotropy during the reorientation process. The related expression reads:[71]

$$\frac{1}{T_1^{\mathrm{lib}}} = g^{(2,0)^2} J_{1,0}(\omega_0) + 2 * g^{(2,2)^2} J_{1,2}(\omega_0), \tag{26}$$

where $g^{(2,0)} = \sqrt{2/3}[g_z - (g_x + g_y)/2]\mu_B B$, $g^{(2,2)} = (g_x - g_y)\mu_B B/2$ are suitable tensor spherical components[58] and $J_{m,n}(\omega_0)$ is the spectral density evaluated at the electron Larmor angular frequency ω_0,

$$J_{l,m}(\omega) = \frac{1}{2}\int_{-\infty}^{-\infty} \langle D_{l,m}^2(0) D_{l,m}^{2*}(t)\rangle \exp(-i\omega t) dt, \tag{27}$$

where $D_{l,m}^2(t)$ is a Wigner matrix describing the rotation to move the molecular frame at time t to the laboratory one.[58]

Several models of the confined rotational motions have been studied.[72–76] Here we adopt the picture discussed by Szabo.[77] He assumes that the molecule rotates around an axis with diffusion coefficient $D_{\parallel}^{\mathrm{lib}}$ and that in turn the latter is wobbling with diffusion coefficient $D_{\perp}^{\mathrm{lib}}$ in a cone of maximum polar angle θ_0. $D_{\parallel}^{\mathrm{lib}}$ and $D_{\perp}^{\mathrm{lib}}$ have expressions being identical to the ones of the usual diffusion model [Eqs. (19) and (20) in the limit of small τ values], i.e., the effect of the confinement does not appear explicitly. Differently, on decreasing θ_0, the rotational correlation times shorten. Due to the weak dependence on $D_{\parallel}^{\mathrm{lib}}$ and to limit the number of adjustable parameters, henceforth the above-mentioned model will be considered in the limit $D_{\parallel}^{\mathrm{lib}} = 0$.

The total spin-lattice relaxation due to both the Raman and the libration processes time reads

$$\frac{1}{T_{1\ i}} = \frac{1}{T_{1\,i}^{\mathrm{Raman}}} + \frac{1}{T_{1\,i}^{\mathrm{lib}}}, \quad i = x,y,z. \tag{28}$$

$T_{1\,i}^{\mathrm{Raman}}$ is the extrapolation of the low-temperature dependence of $T_{1\,i}$ at the temperature of interest. $T_{1\,i}^{\mathrm{lib}}$ is calculated by Eq. (26) by taking the *i*th axis as the cone axis. The model parameters are assumed to be independent of the *i*th axis. This leaves us with two adjustable parameters, the cone angle θ_0 and $D_{\perp}^{\mathrm{lib}}$.

The model is fitted to the spin-lattice relaxation times of K-TEMPO in PI-S10 at $T = 295\ K > T_g$. The best-fit values cover a finite range. Table IV presents some selected results in the range $8.7° < \theta_0 < 20°$. If $\theta_0 < 8.7°$ the amplitude of the libration is too small to relax effectively the longitudinal magnetization and $T_1 \approx T_1^{\mathrm{Raman}}$. If $\theta_0 > 20°$, the reorientation process would lead to appreciable motional averaging of the cw ESR line shape. This was not observed. In fact, our results from cw ESR set an upper limit for θ_0 which is about 10° (Sec. V A). The two best-fit values per each cone angle θ_0 are related to the T_1 minimum when $\omega_0\tau \approx 1$, τ being the correlation time of the fluctuations. When $\theta_0 = 8.7°$ the two values coincide. At this stage we are unable to rule out one of the two solutions which are both listed in Table IV.

TABLE IV. Best-fit of the spin-lattice relaxation times of K-TEMPO in PI-S10 at 295 K according to the confined-motion model with $D_{\parallel}^{\mathrm{lib}} = 0$. The experimental values are $T_{1x} = T_{1y} = 7.5 \pm 0.7\ \mu s$, $T_{1z} = 13.2 \pm 1.3\ \mu s$.

θ_0(deg)	$D_{\perp}^{\mathrm{lib}}$(G s^{-1})	$T_{1x}(\mu s)$	$T_{1y}(\mu s)$	$T_{1z}(\mu s)$
8.7	3.3	6.3	6.9	13.2
14.5	1.84	6.3	6.9	13.3
14.5	50	6.3	6.9	13.3
20	1.91	6.3	6.9	13.2
20	175	6.3	6.9	13.2

Previous ELDOR studies of the reorientation of the spin probe TEMPONE in glassy polymers, i.e., below their glass transition, proved the presence of a fast libration motion of amplitude $\alpha_1 = 4°$ and correlation time $\tau \approx 10$ ps.[25–28] The larger amplitudes listed in Table IV are consistent with these results since they refer to a temperature above T_g where the cage is expected to open up.

Our results from SR compare well with studies on aligned optically active spin probes in glassy polymers, which were found to undergo fast librations in the angular range $5° - 15°$.[32] Furthermore, a recent investigation of the reorientation of polymeric and low molecular-weight glass-formers by ^{2}H-NMR concluded that it is characterized by an amplitude less than 10°.[70]

The larger contribution to $1/T_1$ of the librational motion above T_g is due to either the increase of the amplitude or the faster motion with respect to the glassy phase. The spin-lattice relaxation data do not allow one to discriminate between the two possibilities. However, a coupling of the fast libration dynamics with the structural relaxation is hardly expected due to the wide time scale separation at T_g. On this basis we are more inclined to ascribe the shortening of T_1 above T_g to the increased amplitude of the librations as a consequence of the cage opening. The conclusion agrees with recent NMR results on organic glass-formers.[70] It is also corroborated by the results of the next section which will show that, according to the ESE experiment, there is no coupling of the transverse relaxation time T_2 with the structural arrest occurring at the glass transition. The ESE experiment observes how the average orientation during the libration changes in the time window T_2.

C. Electron spin echo: Short-time reorientation

The decay of the ESE signal is virtually exponential at all temperatures under study. Figure 10 shows the results at 260 K. The temperature dependence of the transverse relaxation time T_2 is shown in Fig. 11. They did not depend on either the spin probe concentration or the amplitude of the microwave field, ruling out the spin diffusion and the instantaneous diffusion relaxation mechanisms.[36] Furthermore, the possible magnetization transfer due to the nuclear spin flips should be negligible since it is expected that $T_2 < T_{1N}$.[27,42] The temperature dependence of T_2 is not monotonous. On cooling from room temperature, T_2 first increases, then it decreases by lowering the temperature below about 200 K. An analogous dependence has been found earlier for nitroxide spin probes in other systems.[78,79] It was noted that at low

Downloaded 26 Nov 2003 to 131.114.128.200. Redistribution subject to AIP license or copyright, see http://ojps.aip.org/jcpo/jcpcr.jsp

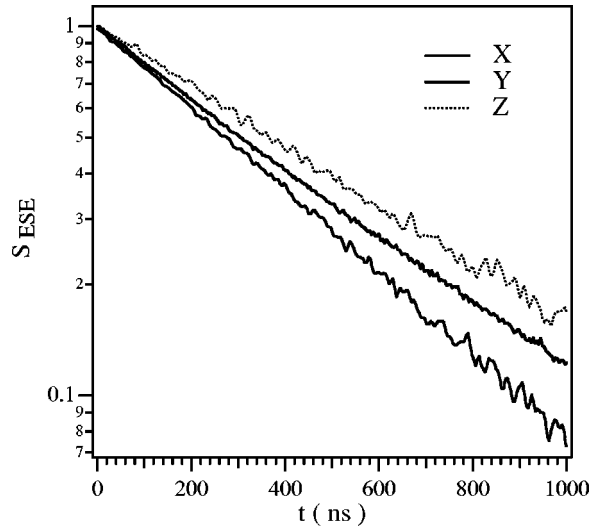

FIG. 10. The decay of the ESE signal of K-TEMPO in PI-S10 at B_x, B_y, and B_z at $T=260$ K. Time t is twice the spacing τ between the first and the second pulse.

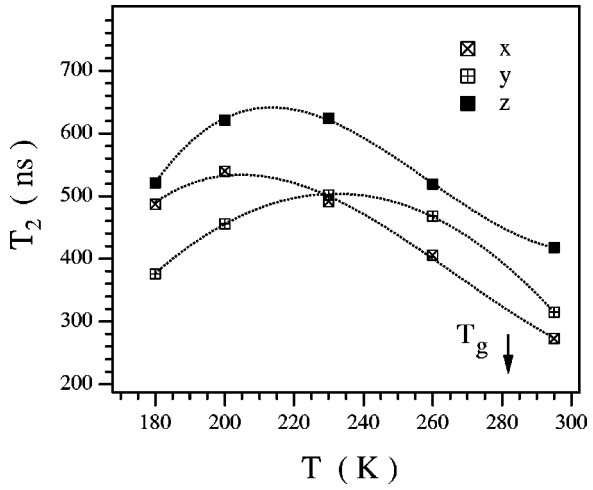

FIG. 11. Temperature dependence of the transverse relaxation time T_2 of K-TEMPO in PI-S10. The dashed lines are guides for the eyes.

temperatures T_2 is mainly affected by the thermally activated rotation of the methyl groups in the nitroxide moiety which modulates the electron-nuclear dipolar interaction with the methyl-group protons. For $T>200$ K the effect is averaged out and T_2 is set by the reorientation process of the spin probe. One remarkable feature of the data shown in Fig. 11 is that no anomaly is observed at T_g. This proves that on the time scale $T_2\approx 500$ ns the reorientation of the spin probe is only weakly coupled to the structural relaxation.

According to the discussions in Secs. V A and V B, the spin probe is not expected to undergo large-angle reorientations on the time scale of T_2. We also note that T_2 exhibits considerable anisotropy also at variance with the presence of large-angle jumps [see Eq. (1)]. On this basis we fitted the T_2 values at the investigated temperatures by using the model detailed in Sec. III A. Only two parameters are adjustable, the diffusion coefficients $D_\parallel$ for rotations of K-TEMPO around the z axis and $D_\perp$ for rotations around the x and y axes (Fig. 5). The results are listed in Table V. The agreement is rather satisfactory even if T_{2y} is overestimated at lower temperatures. We ascribe this to larger contributions by the electron-nuclear dipolar interaction with the methyl-group protons which are not accounted for by the model and the less effective orientation selection at the y position compared to the x and z position (see Fig. 2). The best-fit values fulfill the consistency requirement Eq. (16). In fact, the angular displacement of K-TEMPO during T_{2z}, i.e., the longer observation time of the ESE experiment, is small. From Eqs. (19) and (20) we get $\delta\theta=3°$, $\delta\phi=3.3°$ at 260 K. These angular displacements change the resonance fields less than 0.1 mT at $B_{x,y,z}$, i.e., less than the excitation bandwidth of the pulses. This means that virtually all the excited spins are refocused by the second pulse of the ESE sequence, as is assumed by the model presented in Sec. III A.

The motion observed by ESE may be pictured as a slower reorientation of the average orientation of the spin probe while undergoing the fast libration motion that dominates T_1 above T_g. The above-noted results suggest that this process may be conveniently described as anisotropic free diffusion when it covers angular ranges of about $3°-4°$. The conclusion agrees with the results from cw-ESR that the probe is confined to angular displacements θ_0, $\phi_0<10°$ over time intervals of about 50 ns. It is important to understand if this conclusion is robust or model-dependent. To this aim, we repeated the analysis of the ESE data to see whether they fit to the model describing the motion as confined in a cone of width θ_0 (see Sec. V B). T_2 is evaluated in the same spirit of Sec. V B, i.e., according to the Redfield relaxation theory. The general expressions in terms of the spectral densities $J_{l,m}(\omega)$ are well known and derived elsewhere.[39] Particular spectral densities for the case at hand are evaluated by the expressions of the rotational correlation functions given in Ref. 77. In the dynamical regime under investigation the basic assumption of the Redfield theory, i.e., T_2 is much longer than the rotational correlation times, is fulfilled. T_{2i} is calculated by taking the ith axis as the cone axis. For simplicity reasons, the three adjustable parameters of the model $D_\perp^W$, $D_\parallel$, and θ_0 (one more than the diffusion model) are

TABLE V. Comparison between the transverse relaxation time T_2 of K-TEMPO in PI-S10 and their best-fit $\mathcal{T}_2$ according to Eqs. (13)–(15) in terms of $D_\parallel$ and $D_\perp$.

T (K)	T_{2x}(ns)	T_{2y}(ns)	T_{2z}(ns)	$\mathcal{T}_{2x}$(ns)	$\mathcal{T}_{2y}$(ns)	$\mathcal{T}_{2z}$(ns)	$D_\parallel(s^{-1})$	$D_\perp(s^{-1})$
200	540±1	456±2	621±3	540	696	621	1070	944
230	491±1	503±2	624±3	492	617	624	1725	935
260	406±1	468±2	519±10	387	479	519	3200	1350
295	273±6	315±3	424±12	267	317	430	9600	1960

Downloaded 26 Nov 2003 to 131.114.128.200. Redistribution subject to AIP license or copyright, see http://ojps.aip.org/jcpo/jcpcr.jsp

taken to be independent of the direction of the cone axis. Since the parameters $D_{\perp}^{W}$, $D_{\parallel}$ have no explicit dependence on the confinement, we first try to adjust only θ_0 and take $D_{\perp}^{W}$, $D_{\parallel}$ from the best-fit values of Table V. The agreement is poor, e.g., at 295 K the best fit is obtained for $\theta_0=5.0°$ yielding $\mathcal{T}_{2x}=$ 211 ns, $\mathcal{T}_{2y}=278$ ns, $\mathcal{T}_{2z}=560$ ns. Adjusting all three parameters leads to significant improvement for larger cone angles. For $\theta_0=13.5°$, $D_{\perp}^{W}=9.1\times10^{5}$ s^{-1}, $D_{\parallel}=8.2\times10^{7}$ s^{-1} the best-fit values are $\mathcal{T}_{2x}=272$ ns, $\mathcal{T}_{2y}=327$ ns, $\mathcal{T}_{2z}=424$ ns. The quality of the fit is comparable to our model (see Table V). At 260 K the choice $\theta_0=12.6°$, $D_{\perp}^{W}=9.1\times10^{5}$ s^{-1}, $D_{\parallel}=1.4\times10^{8}$ s^{-1} yields the best-fit values $\mathcal{T}_{2x}=408$ ns, $\mathcal{T}_{2y}=475$ ns, $\mathcal{T}_{2z}=516$ ns which are rather satisfactory (see Table V). At both 295 and 260 K the best fit gives correlation times being shorter than T_2. We did not carry out the analysis at lower temperatures since the effect of the methyl group rotation becomes important.

The above-presented analysis shows that, in order to fit the ESE data, the cone model needs relatively large cone angles $\theta_0\approx13°$ and fast motion of the wobbling axis. These dynamical features would lead to non-negligible narrowing effects in the cw ESR line shape. As there is no evidence for such broadening in the experimental cw EPR spectra, we may set an upper limit $\theta_0<10°$ at variance with the cone model (see Sec. V A). However, we do not consider this as a conclusive argument to finally dismiss the cone model.

A firm decision for or against the cone model can be based on complementing the ESE experiment with other experiments. In fact, the additional information provided by the SE experiment proves that the cone model is not consistent (see the next section). This puts lower limits on the cage size which, on the basis of our ESE analysis in terms of the diffusion model, are $\theta_0,\phi_0>3°$ at 260 K. This must be compared with the results from cw ESR ($\theta_0,\phi_0<10°$).

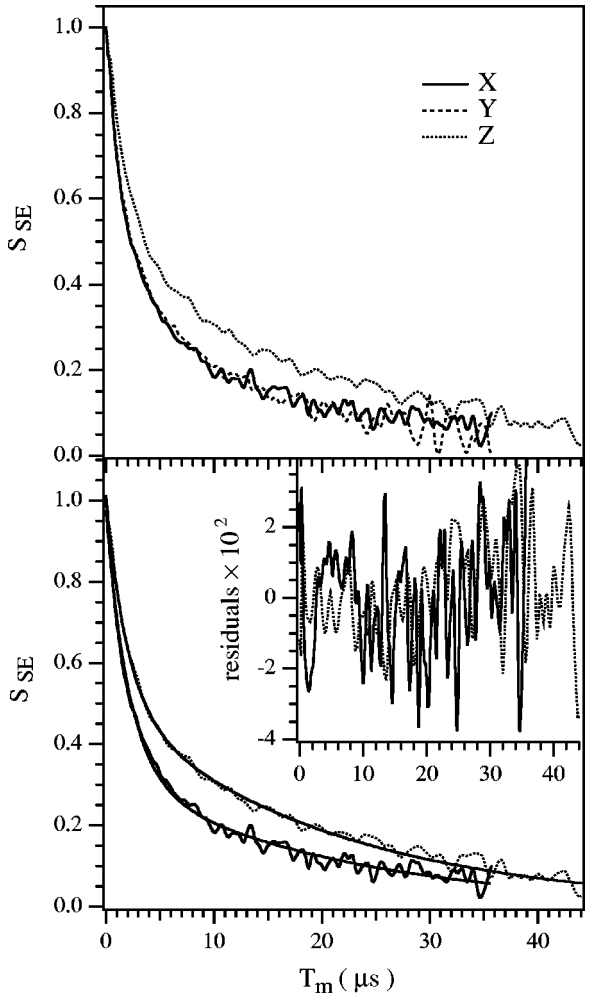

FIG. 12. Top: the decay of the SE signal at B_x, B_y, and B_z by increasing the mixing time T_m. $T=230$ K ($t_p=100$ ns, $\tau=3t_p$). Bottom: comparison between the SE signal at B_x and B_z and the best fit with a weighted sum of two decaying exponentials. The inset shows the residuals. The best-fit parameters are listed in Table VI.

D. Stimulated echo: Long-time reorientation

For the present sample the SE experiment is feasible only below T_g where both T_2 and T_1 are sufficiently long to get good signal-to-noise ratio and provide limited contribution to the decay time. Figure 12 shows the SE decay at B_x, B_y, and B_z observed when increasing the mixing time T_m at 230 K. The damping due to the spin-lattice relaxation has been removed according to the procedure of Sec. IV. The decays are fitted by a weighted sum of two exponentials with decay times τ_{SE} and T_{SE} and weights $w_{T_{\mathrm{SE}}}$, $w_{\tau_{\mathrm{SE}}}$. The best-fit results are listed in Table VI. We notice that the slowest component has larger weight and decay times T_{SE} which are at least about one order of magnitude longer than the other component.

The fast component is due to the initial decay of the transverse magnetization on the time scale of about T_2 (Fig. 11), which can be more easily characterized by the ESE experiment. In contrast to the time scale of the slow decay, this time scale is not well separated from the time required for building up the grating of the longitudinal magnetization (Fig. 3) and therefore cannot be simply expressed by the physically intuitive correlation function given by Eq. (17). To analyze the short-time regime of the SE decay, one would have to resort to a quantum-mechanical evaluation of the time evolution of the full density matrix including not only the mixing period of the SE sequence, as Eq. (17) does, but also the evolution and the detection ones. While this would be possible in principle, it would be much more complicated than our current approach and would provide only limited new insight. In fact, the information which may be collected by the SE fast decay is nothing but the one which is gathered by the ESE experiment, the latter has a much better signal-to-noise ratio (the pulse sequence involves one pulse less than the SE), is easier to analyze, and the ESE-like fast component of the SE signal is almost three times at least less intense than the slow one. Furthermore, in the following it will be shown that the reorientation of the spin probe on the time scales T_2 and T_{SE} ($T_{\mathrm{SE}}/T_2>10$) has different characters. This would require a more elaborate model of the rotational dynamics to describe the SE decay at both short and long time scales. In view of the above remarks we limit the discussion to the slow component of the SE decay. It covers time scales which are about two orders of magnitudes longer

Downloaded 26 Nov 2003 to 131.114.128.200. Redistribution subject to AIP license or copyright, see http://ojps.aip.org/jcpo/jcpcr.jsp

TABLE VI. Best-fit results of the stimulated-echo signal at the three canonical orientations according to a weighted sum of two decaying exponentials with decay times τ_{SE} and T_{SE}. The ratio of the weights of the two components $r = w_{T_{SE}}/w_{\tau_{SE}}$ is also listed.

T (K)	r_x	$\tau_{SE\,x}(\mu s)$	$T_{SE\,x}(\mu s)$	r_y	$\tau_{SE\,y}(\mu s)$	$T_{SE\,y}(\mu s)$	r_z	$\tau_{SE\,z}(\mu s)$	$T_{SE\,z}(\mu s)$
180	2.3±0.2	2.0±0.2	18±2	2.3±0.2	1.6±0.2	18±1	2.9±0.2	1.7±0.2	43±5
200	2.4±0.2	2.3±0.2	18±2	2.4±0.2	2.3±0.2	18±2	3.1±0.2	2.3±0.2	43±2
230	2.4±0.2	1.8±0.2	18±2	2.4±0.2	1.6±0.2	18±2	3.1±0.2	1.7±0.2	43±2
260	2.6±0.2	1.2±0.2	14±2	2.6±0.2	1.3±0.2	16±2	3.1±0.2	1.2±0.2	33.8±2

than the ESE experiment. The decay is due to two different processes, the nuclear spin transitions and the spectral diffusion, i.e., the change of the resonance frequency following the reorientation of the spin probe. The fact that the spin-lattice relaxation times are still strongly anisotropic even after the initial 40-μs-long saturating pulse (Fig. 9) suggests that the role played by the nuclear spin transitions is not dominant. This conclusion is corroborated by other observations as well. Figure 13 shows the time-domain shape of both the real and the imaginary parts of SE at B_z. On increasing the mixing time, the real part narrows and the imaginary part increases. These effects cannot be explained in terms of the nuclear spin transitions. Instead, they suggest that the spin probe undergoes small-angle reorientation on time scales comparable to 10 μs. This motion on one side broadens the frequency distribution of the excited spin probes and on the other side makes it more asymmetric due to the initial excitation at one of the extrema of the overall distribution.

To assess the role of the nuclear-spins transitions, we also studied how the SE decay time depends on the number of lobes of the grating pattern which is roughly given by $2\tau/t_p+1$ (see Fig. 3). Figure 14 shows that the decay time shortens with an increasing number of lobes. If the nuclear spin flips drive the SE relaxation, no dependence of the decay time on the ratio τ/t_p is expected. In contrast, a decay due to small-angle reorientation becomes more effective if the grating is finer [Eq. (17)].

The above-mentioned findings lead to the conclusion that SE decay is mainly driven by the spectral diffusion and in a preliminary way that the latter results from small-angle reorientation at long time scales. Before we discuss the latter issue, we turn our attention to the additional information which may be drawn from the SE experiment on shorter time scales which were investigated by SR and ESE.

The signal-to-noise ratio of SE is rather poor at 290 K. This is consistent with SR results pointing out that at 290 K the fast librations of the spin probe cover a range of about 10° suffices to make SE vanishingly small (see Sec. III B). Obviously, also other reorientation processes may damp the SE amplitude effectively.

The analysis of the ESE signal was carried out in terms of two models, the usual anisotropic diffusion model and the cone model, describing the confined reorientation in a cone of width θ_0 (Sec. V C). Both models fit the ESE data in spite

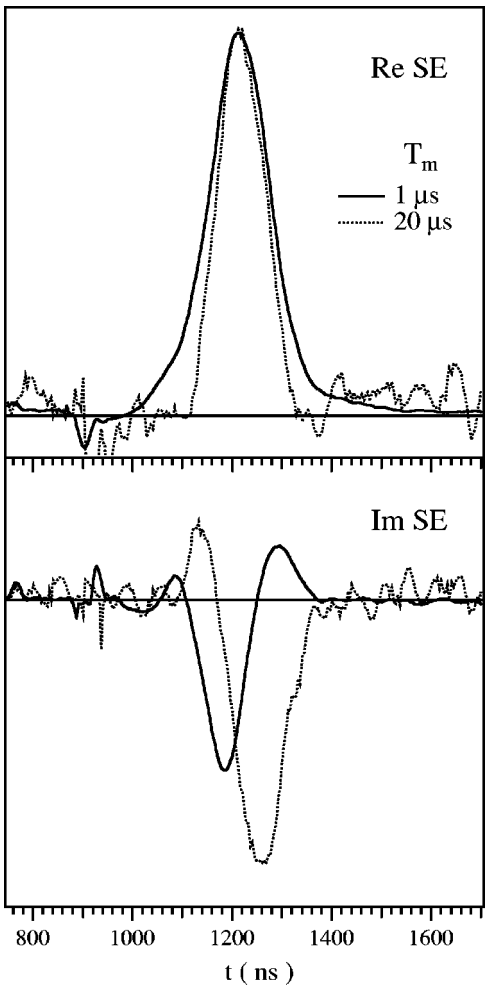

FIG. 13. The real and the imaginary parts of the stimulated echo at B_z for two different mixing times T_m ($T=230$ K, $t_p=100$ ns, $\tau=3t_p$).

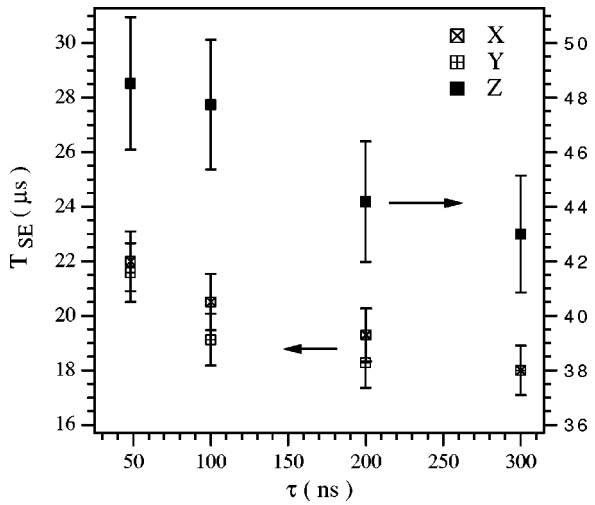

FIG. 14. The dependence of the decay time of the stimulated echo at B_x, B_y, and B_z on the spacing between the first and the second pulse τ at 230 K, $t_p=100$ ns.

Downloaded 26 Nov 2003 to 131.114.128.200. Redistribution subject to AIP license or copyright, see http://ojps.aip.org/jcpo/jcpcr.jsp

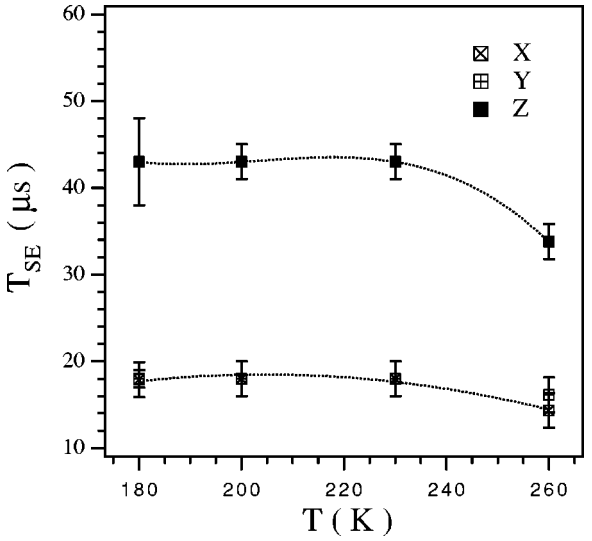

FIG. 15. Temperature dependence of the decay time of the stimulated echo T_{SE} for K-TEMPO in PI-S10 ($\tau = 3t_p$). The dashed lines are guides for the eyes. $t_p = 100$ ns.

of the rather different pictures of the reorientation.

The results of the SE experiment, however, are not consistent with the cone model. The conclusion is reached by considering the evolution period of the SE sequence, i.e., the lapse of time between the first and the second pulse. It covers a time interval which is about three times less than T_2. Then, any dynamical model to fit the ESE data must account for the reorientation during the evolution period as well. The cone model provides the best fits of T_2 with $\theta_0 \approx 13°$ and diffusion coefficients $D_\perp^W \approx 10^6\ s^{-1}$. Accordingly, the spin probe would take a few nanoseconds to span the angular range of few degrees [see Eq. (20)]. Since the evolution period is longer than 100 ns this process would prevent the buildup of the population grating. Consequently, the SE signal would have very small amplitude and decay times T_{SE} about four orders-of-magnitude faster than the experimental values (see Fig. 15). The usual diffusion model (with one adjustable parameter less than the cone model) does not suffer the same flaw. The best-fit values of the diffusion coefficients are three-to-five orders of magnitude smaller than that of the cone model (see Table V). After the longest evolution period $\tau = 300$ ns of the SE sequence, i.e., the spacing between the first and the second pulse, the angular displacement is less than 2° at 260 K and even smaller at the lowest temperatures. Proper MC simulations based on the model of Sec. III B prove that such small angular displacements do not prevent the grating formation (Fig. 3).

In the following, we discuss if the reorientation process observed on the time scale $T_2 \approx 500$ ns and described by the diffusion model also accounts for the SE decay which is one to two orders of magnitude longer.

In Fig. 15 the temperature dependence of the decay time T_{SE} is plotted. It is noted that it is rather weak below T_g. This is different from what is observed on the shorter time scale of T_2 (Fig. 11). We also note that the reorientation process has some uniaxial feature, in that $T_x^{SE} \cong T_y^{SE} < T_z^{SE}$.

The different temperature behavior of T_2 and T_{SE} suggests that the reorientation process detected by the ESE experiment is not responsible for the much slower SE decay which is observed on increasing T_m. In fact, if K-TEMPO reorients as it is observed by ESE, it takes about 1 and 2 μs at 260 and 200 K, respectively, to achieve angular displacements $\delta\theta$ and $\delta\phi$ as large as 4° [see Eqs. (19), (20) and Table V]. Such changes are large enough to damp the SE decay (see Sec. III B). Then, one estimates $T_{SE} \cong 2\ \mu s$ which is fairly shorter than the actual values (Fig. 15). We conclude that on the short time scale $T_2 < 1\ \mu s$ the reorientation process spans small angular regions ($\delta\theta \cong \delta\phi \cong 3°$ at 260 K) and is faster than the one observed at longer time scales $T_{SE} > 10\ \mu s$.

We ascribe this to the increasing constraints acting on the spin probe during its long-time reorientation. In fact, the spin probe rotation occurs in the presence of proper rearrangements of the surroundings.[29] At low temperatures, there is a large number of independent but localized rearranging regions, and rearrangements in each region involve only a small (of order unity) subset of particles.[80,81] This implies that in the short-time regime, which is sensed by the ESE experiment, only low energy barriers are overcome. At longer times, rearrangements occur only if the involved, mutually independent, rearranging regions fulfill certain configurational constraints. This feature is usually described in terms of proper entropic barriers.[80–82] Below T_g the subsequent long-time motion is slow and temperature-independent. The above-presented picture provides a consistent combined interpretation of the results drawn by the ESE and SE experiments.

We now analyze the reorientation as observed by the SE experiment in terms of our MC model (Sec. III B).

The fit of the SE decay times T_{SE} by the MC model has four adjustable parameters, $\Delta\theta$, $\Delta\phi$, τ_θ, τ_ϕ, i.e., the jump sizes and the the waiting-times between jumps. The SE decays are anisotropic, $T_{SE\,x} \cong T_{SE\,y} < T_{SE\,z}$. According to the discussion of Sec. III B, it implies that $\Delta\phi$ is small ($\Delta\phi < 10°$) and $\tau_\theta > \tau_\phi$. When adjusting the four parameters of the MC model to fit the three SE decay-times values, a unique set of best-fit values is not found. The issue deserves a careful discussion.

The results of Sec. III B prove that SE is largely affected by the occurrence of even a single θ jump irrespective of its size. This means that T_{SE} is set by the probability that at least one jump occurs during the lapse of time T_{SE}. The latter is controlled by the magnitude of τ_θ. Henceforth, T_{SE} is not very sensitive to the magnitude of $\Delta\theta$.

To characterize the set of the best-fit triples $\{\Delta\phi, \tau_\phi, \tau_\theta\}$, at first one sets $\tau_\theta \to \infty$ in the MC runs. This corresponds to a dynamic regime with no appreciable θ changes within the observation time T_{SE}. The best-fit results are listed in Table VII. It is seen that changing the temperature requires the adjustment of τ_ϕ only. This is expected in glassy environments where, on changing the temperature, only the time scales of the dynamics are changed with almost no structural changes.

The best-fit triples with $\Delta\theta \neq 0$, or equivalently finite τ_θ values, are found by trial and error. Initial guesses are provided by Eq. (23). One notes that $\mathcal{T}_{SE\,x,y}|_{\Delta\theta=0} \cong \tau_\phi$ (see

Downloaded 26 Nov 2003 to 131.114.128.200. Redistribution subject to AIP license or copyright, see http://ojps.aip.org/jcpo/jcpcr.jsp

TABLE VII. Comparison between the stimulated-echo decay time T_{SE} of K-TEMPO in PI-S10 and the best-fit $\mathcal{T}_{SE}$ from the Monte Carlo simulations. $\tau_\theta \to \infty$. $t_p = 100$ ns, $\tau = 3t_p$.

T (K)	$T_{SE\,x}(\mu s)$	$T_{SE\,y}(\mu s)$	$T_{SE\,z}(\mu s)$	$\mathcal{T}_{SE\,x}(\mu s)$	$\mathcal{T}_{SE\,y}(\mu s)$	$\mathcal{T}_{SE\,z}(\mu s)$	$\Delta\phi$(deg)	$\tau_\phi(\mu s)$
180	18±2	18±1	43±5	18	19	43	7.7	19.4
200	18±2	18±2	43±2	18	19	43	7.7	19.4
230	18±2	18±2	43±2	19	20	44.9	7.7	20.7
260	14±2	16±2	33.8±2	14.3	15.8	33.5	7.7	15.3

Table I) and $\mathcal{T}_{SE\,z}|_{\Delta\theta=0} = \tau_\phi f(\Delta\phi)$, while $f(\Delta\phi)$ is numerically known from the MC results. Replacing these relations into Eq. (23) with the guesses $\tilde{\mathcal{T}}_{SE\,x,y} \cong (T_{SE\,x} + T_{SE\,y})/2$ and $\tilde{\mathcal{T}}_{SE\,z} \cong T_{SE\,z}$ allows one to relate τ_ϕ and τ_θ to $\Delta\phi$. If needed, additional MC runs refine the guesses to get the best-fit values. Figure 16 plots the guesses for the SE data at $T = 260$ K. The situation for the other temperatures is quite similar. The effectiveness of the above-noted procedure is appreciated by comparing: (i) the best-fit results at $T = 260$ K in Table VII with the guesses of $\Delta\phi$ and τ_ϕ when τ_θ diverges in Fig. 16, (ii) the limit values of τ_ϕ and τ_θ in Fig. 16 when $\Delta\phi$ vanishes with the expected values given by Eq. (25). As a matter of fact, the guesses provided by the above-noted scheme are found to be rather close to the best-fit results provided by the MC model. This is not surprising in view of the effectiveness of Eq. (23) pointed out in Sec. III B.

Figure 16 captures the basic features of the long-time reorientation of K-TEMPO which hold at lower temperatures, too. On average, ϕ jumps have amplitude $\Delta\phi < 8°$ with average waiting time $\tau_\phi \approx \mathcal{T}_{SE\,x,y} \cong T_{SE\,x,y}$. The amplitude of θ jumps is unknown, they are slower than ϕ jumps with average waiting time τ_θ, which is longer than $\mathcal{T}_{SE\,z} \cong T_{SE\,z}$.

By using Eq. (19) we may give an upper bound of the long-time diffusion coefficient of the ϕ angle, $D_\parallel^{SE}$ from Table VII. In fact, the table assumes $\tau_\theta \to \infty$ and, if the latter is finite, the data are consistent with slower ϕ reorientation (see Fig. 16). One finds $D_\parallel^{SE}$ 590 s^{-1} at 260 K and 465 s^{-1} at 180 K. A comparison with the corresponding quantity describing the reorientation of the ϕ angle on the shorter T_2 time scale (Table V) shows that the latter is faster. This points to the conclusion that the reorientation process of the spin probe, as detected by SE, is slower than the one detected by ESE on shorter time scales.

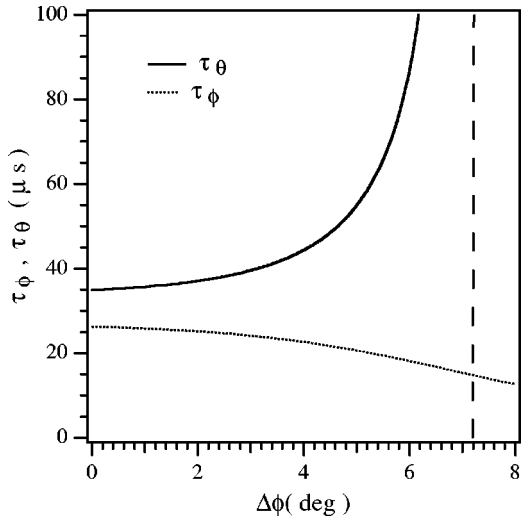

FIG. 16. Initial guesses τ_θ and τ_ϕ plotted as functions of $\Delta\phi$ for the best fit of the SE decay times of K-TEMPO in PI-S10 at 260 K. The guesses are derived according to the procedure detailed in Sec. V D. The dashed vertical line marks the $\Delta\phi$ value where τ_θ diverges.

VI. CONCLUSIONS

We investigated the reorientation of a spin probe strongly localized close to the ionic clusters of an ionomer by continuous wave and pulsed high-field ESR. The investigation profited from the excellent orientation resolution of high-field ESR and covered the dynamic range from the picosecond up to the microsecond time scale in the glass transition region of the polymer ($0.64 < T/T_g < 1.05$). Simple relations were found between the parameters of an anisotropic diffusion model, on the one hand, and the transverse relaxation time T_2 as well as the decay time of the stimulated echo, on the other hand, by restricting analysis to the canonical orientations.

The analysis of the cw-ESR line shape shows that the changes of the ϕ and θ angles describing the orientation of the spin probe are smaller than $\phi_0 \cong \theta_0 \cong 10°$ for correlation times of about 50 ns. Large-angle reorientation can occur only with much longer correlation times.

The SR experiment provides information on the spin lattice relaxation time T_1, which is sensitive to the very fast dynamics occurring at frequencies close to the Larmor frequency $\nu_0 = 94$ GHz. In the glassy regime, T_1 is dominated by intramolecular Raman processes whereas above T_g a new regime is observed, which is ascribed to the fast libration of the spin probe in the wider cage where it is hosted.[70] At $T/T_g = 1.05$ the analysis yields libration angles in the range $8.7° - 10°$. Larger libration angles would lead to appreciable motional narrowing of the cw ESR line shape at variance with the experimental findings.

The reorientation at short time scales has been investigated by ESE which has observation times about $T_2 \cong 500$ ns. To interpret the results, an analytical model has been developed which profits from the small angular range spanned by the spin probe during T_2. The available ESE data are unable to discriminate between quite different reorientation models. By complementing these data with data from the SE experiment, it was found that consistent results are obtained only by using the rotational diffusion model. This implies that no remarkable trapping effect occurs when the spin probe motion spans $3° - 4°$ angular ranges. In the

Downloaded 26 Nov 2003 to 131.114.128.200. Redistribution subject to AIP license or copyright, see http://ojps.aip.org/jcpo/jcpcr.jsp

investigated temperature range the diffusion coefficients are in the range 10^3-10^4 s^{-1}. Crossing the glass transition temperature does not lead to any observable effect. On the T_2 time scale, the reorientation of the spin probe is thus interpreted as due to local rearrangements of the cage with poor coupling to the structural relaxation.

At longer time scales the reorientation has been investigated by SE whose observation time is about $T_{SE}\cong 10-40$ μs. On this time scale T_{SE} and the reorientation do not exhibit appreciable temperature dependence below the glass transition temperature. This has been explained by the increasing constraints acting on the spin probe during its long-time reorientation. The experimental results have been compared to Monte Carlo simulations describing the random motion of the orientation (ϕ,θ) in terms of jump dynamics. On average, ϕ jumps have amplitude $\Delta\phi<8°$ with average waiting time $\tau_\phi\approx T_{SE\,x,y}$. The amplitude of θ jumps remains unknown, they are slower than ϕ jumps with an average waiting time which is longer than $T_{SE\,z}$. Upper bounds of the long-time diffusion coefficient of the ϕ angle, $D_\parallel^{SE}$, are 590 s^{-1} at 260 K and 465 s^{-1} at 180 K, i.e., fairly less than the corresponding quantities measured by ESE.

The present study clearly shows that a hierarchy of dynamic processes exists. The spin probe undergoes fast intramolecular librations on the time scale of a few picoseconds, experiences the local rearrangement of the cage on the time scale of about hundreds of nanoseconds, and performs cooperative reorientation over time scales comparable to or longer than several microseconds in the glass transition region.

ACKNOWLEDGMENTS

Financial support by the DFG Schwerpunkt ''Polyelektrolyte'' and the DFG Schwerpunkt ''Hochfeld-EPR in Biologie, Chemie und Physik'' is gratefully acknowledged. The authors thank A. Eisenberg, S. Eaton, G. Eaton, and A. Kh. Vorobiev for helpful discussions.

APPENDIX A: EXPANSION COEFFICIENTS

The explicit expression of the coefficients in the expansions (10), (11), and (12) are derived by Eqs. (3) and (4) and read as

$$f_{0\,x}=\frac{1}{3}\left\{\gamma_x'+\frac{M}{2A_xg_x^2}[2(A_z^2-A_x^2)g_z^2-(A_y^2-A_x^2)g_y^2]\right\}, \tag{A1}$$

$$f_{0\,y}=\frac{1}{3}\left\{\gamma_y'+\frac{M}{2A_yg_y^2}[2(A_z^2-A_y^2)g_z^2-(A_x^2-A_y^2)g_x^2]\right\}, \tag{A2}$$

$$f_{0\,z}=\frac{1}{3}\left\{\gamma_z'+\frac{M}{2A_zg_z^2}[(A_z^2-A_x^2)g_x^2+(A_z^2-A_y^2)g_y^2]\right\} \tag{A3}$$

with $\gamma_i'=\mu_BB[2g_z^2-(g_x^2+g_y^2)]/2g_i$ and

$$\eta_x=\frac{1}{f_{0\,x}}\left\{\gamma_x''+\frac{A_x^2-A_y^2}{2A_x}\frac{g_y^2}{g_x^2}M\right\}, \tag{A4}$$

$$\eta_y=\frac{1}{f_{0\,y}}\left\{\gamma_y''+\frac{A_x^2-A_y^2}{2A_y}\frac{g_x^2}{g_y^2}M\right\}, \tag{A5}$$

$$\eta_z=\frac{1}{f_{0\,z}}\left\{\gamma_z''+\left[\frac{A_x^2-A_z^2}{2A_z}\frac{g_x^2}{g_z^2}-\frac{A_y^2-A_z^2}{2A_z}\frac{g_y^2}{g_z^2}\right]M\right\} \tag{A6}$$

with $\gamma_i''=\mu_BB(g_x^2-g_y^2)/2g_i$. In the limit of small g anisotropy the above-given results reduce to the compact forms $(i=x,y,z)$:

$$f_{0\,i}=\frac{1}{3}\left\{[2g_z-(g_x+g_y)]\mu_BB+\frac{2A_z^2-(A_x^2+A_y^2)}{2A_i}M\right\}, \tag{A7}$$

$$\eta_i=\frac{1}{f_{0\,i}}\left\{(g_x-g_y)\mu_BB+\frac{A_x^2-A_y^2}{2A_i}M\right\}. \tag{A8}$$

APPENDIX B: TRANSVERSE RELAXATION TIMES

We first evaluate T_{2x}. The first pulse of the ESE sequence selects molecules resonating at $\omega(\theta,\phi)=\omega_x+\delta\omega_x$ [Eq. (10)]. ω_x corresponds to the orientation $\theta_0=\pi/2$, $\phi_0=0$. By replacing $y=\rho(\Omega,t)\sqrt{\sin\theta}$ and Fourier-transforming, Eq. (8) reduces to $(i^2=-1)$:

$$\left\{D_\perp\frac{\partial^2}{\partial\theta^2}+i\frac{\eta_x-3}{2}f_{0\,x}\delta\theta^2+D_\parallel\frac{\partial^2}{\partial\phi^2}+i\eta_xf_{0\,x}\delta\phi^2+\frac{D_\perp}{2}+i(\omega-\omega_x)\right\}\hat{y}=-i\sqrt{\sin\theta}. \tag{B1}$$

Equation (B1) is solved by separating the variables θ and ϕ. Then, we have to solve the equations of motion of two uncoupled one-dimensional harmonic oscillators. The real part of the sum of the two lowest eigenvalues yields T_{2x}^{-1}, Eq. (13). Equation (14) for T_{2y} is derived in an analogous way.

Now we turn to the evaluation of T_{2z}^{-1}. The first pulse selects molecules resonating at $\omega(\theta,\phi)=\omega_z+\delta\omega_z$ [Eq. (12)]. ω_z corresponds to the orientation $\theta_0=0$. The explicit expression of the diffusion operator Γ in Eq. (8) includes a term

$$\left[\frac{D_\perp}{\sin^2\theta}+(D_\parallel-D_\perp)\right]\frac{\partial^2}{\partial\phi^2}.$$

It is safe to assume the inequality $\sin^2\theta\ll D_\perp/|D_\parallel-D_\perp|$. In fact, usually $0.1<D_\parallel/D_\perp<10$ requiring $\theta\ll 20°$. The typical angular range spanned in the present study during the relaxation time T_{2z}^{-1} is less than 4°. As a consequence, Eq. (8) takes the form

$$\left\{D_\perp\left[\frac{1}{\theta^2}\frac{\partial^2}{\partial\phi^2}+\frac{1}{\theta}\frac{\partial}{\partial\theta}+\frac{\partial^2}{\partial\theta^2}\right]-i\frac{\eta_z\cos 2\phi-3}{2}f_{0\,z}\delta\theta^2+i(\omega-\omega_z)\right\}\hat{y}=-i, \tag{B2}$$

we replace $u=\theta\cos\phi$, $v=\theta\sin\phi$, and Eq. (B2) becomes

$$\left\{\left[D_\perp\frac{\partial^2}{\partial u^2}+i\frac{3-\eta}{2}f_{0\,z}u^2\right]+\left[D_\perp\frac{\partial^2}{\partial v^2}+i\frac{3+\eta}{2}f_{0\,z}v^2\right]+i(\omega-\omega_z)\right\}\hat{y}=-i. \tag{B3}$$

Downloaded 26 Nov 2003 to 131.114.128.200. Redistribution subject to AIP license or copyright, see http://ojps.aip.org/jcpo/jcpcr.jsp

By separating the variables u and v, we again obtain the equations of motion of two uncoupled one-dimensional harmonic oscillators. The real part of the sum of the two lowest eigenvalues yields T_{2z}^{-1}, Eq. (15).

[1] K. Schmidt-Rohr and H. W. Spiess, *Multidimensional Solid-State NMR and Polymers* (Academic, London, 1994).
[2] A. Hofmann, F. Kremer, E. W. Fischer, and A. Schönhals, in *Disorder Effects on Relaxational Process*, edited by R. Richert and A. Blumen (Springer, Berlin, 1994).
[3] P. Lunkenheimer, A. Pimenov, M. Dressel, Yu. G. Goncharow, R. Böhmer, and A. Loidl, Phys. Rev. Lett. **77**, 318 (1996).
[4] A. Kudlik, Ch. Tschirwitz, S. Benkhof, T. Blochowicz, and E. Rössler, Europhys. Lett. **40**, 649 (1997).
[5] F. Kremer and A. Schönhals, *Broadband Dielectric Spectroscopy* (Springer, Berlin, 2002).
[6] D. J. Plazek and K. L. Ngai, *AIP Polymer Property Handbook*, edited by J. E. Mark (American Institute of Physics, New York, 1996).
[7] Y. S. Bay and M. D. Fayer, Phys. Rev. B **39**, 11066 (1989).
[8] L. R. Narasimhan, Y. S. Bai, M. A. Dugan, and M. D. Fayer, Chem. Phys. Lett. **176**, 335 (1991).
[9] C. A. Angell, K. L. Ngai, G. B. McKenna, P. F. McMillan, and S. W. Martin, J. Appl. Phys. **88**, 3113 (2000).
[10] *Proceedings of the Second Workshop on Non-Equilibrium Phenomena in Supercooled Fluids, Glasses and Amorphous Materials*, edited by M. Giordano, D. Leporini, and M. P. Tosi [J. Phys.: Condens. Matter **11,** entire issue (1999)].
[11] M. D. Ediger, Annu. Rev. Phys. Chem. **51**, 99 (2000).
[12] R. Richert, Phys. Chem. Condens. Matt. **14**, R703 (2002).
[13] A. Kasper, E. Bartsch, and H. Sillescu, Langmuir **14**, 5004 (1998).
[14] B. Doliwa and A. Heuer, Phys. Rev. Lett. **80**, 4915 (1998).
[15] C. Bennemann, C. Donati, J. Baschnagel, and S. C. Glotzer, Nature (London) **399**, 246 (1999).
[16] K. Vollmayr-Lee, W. Kob, K. Binder, and A. Zippelius, J. Chem. Phys. **116**, 5158 (2002).
[17] S. Kamath, R. H. Colby, S. K. Kumar, and J. Baschnagel, J. Chem. Phys. **116**, 865 (2002).
[18] W. Kob, J. Phys.: Condens. Matter **11**, R85 (1999).
[19] E. Rabani, J. D. Gezelter, and B. J. Berne, J. Chem. Phys. **107**, 6867 (1997).
[20] C. De Michele and D. Leporini, Phys. Rev. E **63**, 036701 (2001); **63**, 036702 (2001).
[21] W. Götze, J. Phys.: Condens. Matter **11**, A1 (1999).
[22] S.-H. Chong and M. Fuchs, Phys. Rev. Lett. **88**, 185702 (2002).
[23] A. Rivera, C. León, C. P. E. Varsamis, G. D. Chryssikos, K. L. Ngai, C. M. Roland, and L. J. Buckley, Phys. Rev. Lett. **88**, 125902 (2002).
[24] D. M. Jacobs, M. D. Zeidler, and O. Kanert, J. Phys. Chem. A **101**, 5241 (1997).
[25] G. G. Maresch, M. Weber, A. A. Dubinskii, and H. W. Spiess, Chem. Phys. Lett. **193**, 134 (1992).
[26] A. A. Dubinskii, G. G. Maresch, and H. W. Spiess, J. Chem. Phys. **100**, 2437 (1994).
[27] J. W. Saalmueller, H. W. Long, G. G. Maresch, and H. W. Spiess, J. Magn. Reson. A **117**, 193 (1995).
[28] J. W. Saalmueller, H. W. Long, T. Volkmer, U. Wiesner, G. G. Maresch, and H. W. Spiess, J. Polym. Sci., Part B: Polym. Phys. **34**, 1093 (1996).
[29] A. Polimeno and J. H. Freed, J. Phys. Chem. **99**, 10995 (1995).
[30] D. J. Xu, R. H. Crepeau, C. K. Ober, and J. H. Freed, J. Phys. Chem. **100**, 15873 (1996).
[31] I. A. Shkrob, B. M. Tadjikov, S. D. Chemerisov, and A. D. Trifunac, J. Chem. Phys. **111**, 5124 (1999).
[32] A. Kh. Vorobiev, V. S. Gurman, and T. A. Klimenko, Phys. Chem. Chem. Phys. **2**, 379 (2000).
[33] D. Leporini, V. Schädler, U. Wiesner, H. W. Spiess, and G. Jeschke, J. Non-Cryst. Solids **307–310**, 510 (2002).
[34] M. A. Ondar, O. Y. Grinberg, L. G. Oranskii, V. I. Kurochkin, and Y. L. Lebedev, J. Struct. Chem. **22**, 626 (1981).
[35] D. E. Budil, K. A. Earle, and J. H. Freed, J. Phys. Chem. **97**, 1294 (1993).
[36] A. Schweiger and G. Jeschke, *Principles of Pulse Electron Paramagnetic Resonance* (Oxford University Press, Oxford, 2001).
[37] V. Schädler, J. Spickermann, H. J. Räder, and U. Wiesner, Macromolecules **29**, 4865 (1996).
[38] V. Schädler, A. Franck, U. Wiesner, and H. W. Spiess, Macromolecules **30**, 3832 (1997).
[39] *Spin Labeling: Theory and Applications*, edited by L. J. Berliner (Academic, New York, 1976); *Biological Magnetic Resonance*, edited by L. J. Berliner and J. Reuben (Plenum, New York, 1989), Vol. 8.
[40] D. Leporini, X. X. Zhu, M. Krause, G. Jeschke, and H. W. Spiess, Macromolecules **35**, 3977 (2002).
[41] See the papers by J. S. Hyde and I. M. Brown, in *Time-domain Electron Spin Resonance*, edited by L. Kevan and R. N. Schwartz (Wiley, New York, 1979).
[42] D. A. Haas, T. Sugano, C. Mailer, and B. H. Robinson, J. Phys. Chem. **97**, 2914 (1993).
[43] J.-L. Du, G. R. Eaton, and S. S. Eaton, J. Magn. Reson. A **115**, 213 (1995).
[44] Y. Zhou, B. E. Bowler, G. R. Eaton, and S. S. Eaton, J. Magn. Reson. **139**, 165 (1999).
[45] S. S. Eaton, J. Harbridge, G. A. Rinard, G. R. Eaton, and R. T. Weber, Appl. Magn. Reson. **20**, 151 (2001).
[46] L. J. Schwartz, A. Stillman, and J. H. Freed, J. Chem. Phys. **77**, 5410 (1982).
[47] A. Baram, Mol. Phys. **44**, 1009 (1981).
[48] D. Kivelson and S. Lee, J. Chem. Phys. **76**, 5746 (1982).
[49] D. Bordeaux, J. Lajzerowicz, R. Briere, H. Lemaire, and A. Rassat, Org. Magn. Reson. **5**, 47 (1973).
[50] W. Smith and L. D. Kispert, J. Chem. Soc., Faraday Trans. 2 **73**, 152 (1977).
[51] A. Abragam and B. Bleaney, *Electron Paramagnetic Resonance of Transition Ions* (Oxford University Press, London, 1970).
[52] *Electron Spin Relaxation in Liquids*, edited by L. T. Muus and P. W. Atkins (Plenum, New York, 1972).
[53] W. B. Mims, K. Nassau, and J. D. Mc Gee, Phys. Rev. **123**, 2059 (1961).
[54] W. B. Mims, Phys. Rev. **168**, 370 (1968).
[55] W. B. Mims, in *Electron Paramagnetic Resonance*, edited by S. Geschwind (Plenum, New York, 1972).
[56] H. W. Spiess, J. Chem. Phys. **72**, 6755 (1980).
[57] R. Kimmich, E. Fischer, P. Callaghan, and N. Fatkullin, J. Magn. Reson. A **117**, 53 (1995).
[58] M. E. Rose, *Elementary Theory of Angular Momentum* (Wiley, New York, 1957).
[59] W. Feller, *An Introduction to Probability Theory and its Applications*, 3rd ed. (Wiley, New York, 1990), Vol. I.
[60] L. Alessi, L. Andreozzi, M. Faetti, and D. Leporini, J. Chem. Phys. **114**, 3631 (2001).
[61] *Ionomers: Characterization, Theory and Applications*, edited by L. Schlick (CRC, New York, 1996).
[62] A. Eisenberg and J.-S. Kim, *Introduction to Ionomers* (Wiley, New York, 1998).
[63] M. Pannier, V. Schädler, M. Schöps, U. Wiesner, G. Jeschke, and H. W. Spiess, Macromolecules **33**, 7812 (2000).
[64] J. S. Hwang, R. P. Mason, L.-P. Hwang, and J. H. Freed, J. Phys. Chem. **79**, 489 (1975).
[65] L. H. Sperling, *Introduction to Physical Polymer Science*, 2nd ed. (Wiley, New York, 1992).
[66] G. G. Cameron, in *Comprehensive Polymer Science, Polymer Characterization* (Pergamon, Oxford, 1989), Vol. I.
[67] M. K. Bowman and L. Kevan in *Time-domain Electron Spin Resonance*, edited by L. Kevan and R. N. Schwartz (Wiley, New York, 1979).
[68] A. Abragam, *Principles of Nuclear Magnetism* (Clarendon, Oxford, 1978).
[69] D. Leporini, V. Schädler, U. Wiesner, H. W. Spiess, and G. Jeschke (unpublished).
[70] M. Vogel and E. Rössler, J. Chem. Phys. **114**, 5802 (2001).
[71] L. Andreozzi, A. Di Schino, M. Giordano, and D. Leporini, Philos. Mag. B **77**, 547 (1998).
[72] C. C. Wang and R. Pecora, J. Chem. Phys. **72**, 5333 (1980).
[73] W. Gronski, Makromol. Chem. **180**, 1119 (1979).
[74] S. P. Van, G. B. Birrell, and O. H. Griffith, J. Magn. Reson. **15**, 444 (1974).
[75] S. A. Dzuba, Yu. D. Tsvetkov, and A. G. Maryasov, Chem. Phys. Lett. **188**, 217 (1992).
[76] S. A. Dzuba, Phys. Lett. A **213**, 77 (1996).
[77] A. Szabo, J. Chem. Phys. **81**, 150 (1984).
[78] S. A. Dzuba, A. G. Maryasov, K. M. Salikhov, and Yu. D. Tsvetkov, J. Magn. Reson. (1969-1992) **58**, 95 (1984).
[79] S. Saxena and J. H. Freed, J. Phys. Chem. A **101**, 7998 (1997).
[80] F. H. Stillinger, Phys. Rev. B **41**, 2409 (1990).
[81] U. Mohanty, I. Oppenheim, and C. Taubes, Science **266**, 425 (1994).
[82] M. Fixman, J. Chem. Phys. **69**, 1527 (1978).

Downloaded 26 Nov 2003 to 131.114.128.200. Redistribution subject to AIP license or copyright, see http://ojps.aip.org/jcpo/jcpcr.jsp